Generation of the Mt Kinabalu granite by crustal contamination of intraplate magma modelled by Equilibrated Major Element Assimilation with Fractional Crystallisation (EME-AFC)

Burton-Johnson, A.[a*], Macpherson, C.G.[b], Ottley, C.J.[b], Nowell, G.M.[b], and Boyce, A.J.[c]

[a]British Antarctic Survey, High Cross, Madingley Road, Cambridge, CB3 0ET, UK

[b]Department of Earth Sciences, University of Durham, Durham, DH1 3LE, UK

[c]Scottish Universities Environmental Research Centre, East Kilbride, G75 0QF, UK

* Corresponding Author

e-mail: alerto@bas.ac.uk

Tel. +44 (0)1223 221284

ABSTRACT

New geochemical data are presented for the composite units of the Mount Kinabalu granitoid intrusion of Borneo and explore discrimination between crustal- and mantle-derived granitic magmas. The geochemical data demonstrate that the units making up this composite intrusion became more potassic through time. This was accompanied by an evolution of isotope ratios from a continental-affinity towards a slightly more mantle-affinity ($^{87}Sr/^{86}Sr_i$ ~0.7078; $^{143}Nd/^{144}Nd_i$ ~0.51245; $^{206}Pb/^{204}Pb_i$ ~18.756 for the oldest unit compared to $^{87}Sr/^{86}Sr_i$ ~0.7065, $^{143}Nd/^{144}Nd_i$ ~0.51250 and $^{206}Pb/^{204}Pb_i$ ~18.721 for the younger units). Oxygen isotope ratios (calculated whole-rock $\delta^{18}O$ of +6.5–9.3‰) do not show a clear trend with time. The isotopic data indicate that the magma cannot result only from fractional crystallisation of a mantle-derived magma. Alkali metal compositions show that crustal anatexis is also an unsuitable process for genesis of the intrusion. The data indicate that the high-K units were generated by fractional crystallisation of a primary, mafic magma, followed by assimilation of the partially melted sedimentary overburden. We present a new, Equilibrated Major Element – Assimilation with Fractional Crystallisation (EME-AFC) approach for simultaneously modelling the major element, trace element, and radiogenic and oxygen isotope compositions during such magmatic differentiation; addressing the lack of current AFC modelling approaches for felsic, amphibole- or biotite-bearing systems. We propose that Mt Kinabalu was generated through low degree melting of upwelling fertile metasomatised mantle driven by regional crustal extension in the Late Miocene.

Key Words

Granite petrogenesis; magma differentiation; AFC modelling; Oxygen isotopes; Borneo

INTRODUCTION

Granitic intrusions form the majority of the Earth's upper continental crust and are commonly associated with precious metal deposits. Understanding their emplacement mechanisms and structure in the crust has evolved from models of slow moving diapirs to rapid, often pulsed, dyke emplacement of laterally extensive laccoliths (e.g. Wiebe, 1988; Clemens & Mawer, 1992; McCaffrey & Petford, 1997; Cruden, 1998; Wiebe & Collins, 1998; Petford & Clemens, 2000; Petford *et al.*, 2000; Vigneresse & Clemens, 2000; de Saint-Blanquat *et al.*, 2006; Vigneresse, 2006; de Silva & Gosnold, 2007; Grocott *et al.*, 2009; Horsman *et al.*, 2009). However, the processes that generate granitic melts remain ambiguous and much debated (e.g. de Fátima Bitencourt *et al.*, 2017; Jagoutz & Klein, 2018).

Three potential mechanisms for producing granitic melts are widely accepted: (i) extreme fractionation of mafic mantle-derived melts; (ii) crustal anatexis; and (iii) mixing of mantle-derived and anatectic melts. Each of these have been proposed for different plutons worldwide (e.g. Bogaerts *et al.*, 2006; Jagoutz *et al.*, 2009; Clemens & Benn, 2010; Chappell & White, 2011; Leuthold *et al.*, 2012). Distinguishing between these processes remains contentious and a fundamental challenge in igneous petrogenesis, but one that is best tackled through a comprehensive geochemical approach.

In this study we present new geochemical data for the Mt Kinabalu pluton of Sabah in Malaysian Borneo. This is an ideal target to study granite petrogenesis because it is composed of units that are mineralogically and geochemically distinct and have ages that are well constrained by both contact relationships and U-Pb zircon dating (Cottam *et al.*, 2010; Burton-Johnson *et al.*, 2017). We show that neither crustal anatexis nor fractionation of mantle-derived melts without crustal involvement

are suitable mechanisms to generate this body. Utilising a new geochemical modelling approach we show that the intrusion's granitic magma was produced by crustal contamination of mantle-derived, intra-plate magma by combined Assimilation and Fractional Crystallisation (AFC) processes.

REGIONAL GEOLOGY

At 4095m elevation, Mt Kinabalu is the highest peak between the Himalayas and Papua New Guinea (Fig. 1a and 1b). The Mt Kinabalu pluton was emplaced in Sabah, NW Borneo, during the late Miocene (Fig. 1c). The region has basement made up of four main components: Jurassic to Cretaceous mafic igneous rocks; Cretaceous radiolarian cherts; variably serpentinised peridotites; and Triassic to Cretaceous rocks, previously described as crystalline basement (Reinhard & Wenk, 1951; Dhonau & Hutchison, 1965; Koopmans, 1967; Kirk, 1968; Leong, 1974; Rangin *et al.*, 1990; Omang, 1993; Swauger *et al.*, 1995; Graves *et al.*, 2000; Hutchison, 2005). These are overlain by a thick cover sequence of predominantly deep-water turbidites and related deposits (Collenette, 1965; van Hattum *et al.*, 2013) of the Cretaceous to Eocene Rajang Group (Sapulut Formation) and the Eocene to Oligocene Crocker Group (including the Trusmadi, Crocker, and Temburong Formations).

The basement and cover sequence were folded and faulted during Eocene and Oligocene deformation driven by the subduction of the proto-South China Sea beneath Borneo (Taylor & Hayes 1983; Rangin & Silver 1990; Tongkul 1991, 1994; Hall 1996; Hall & Wilson 2000; Hutchison 2000). The attenuated South China continental margin collided with northern Borneo in the Early Miocene (Hall & Wilson, 2000; Hutchison, 2000; Hall & Breitfeld, 2017) triggering the Sabah Orogeny (Hutchison, 1996). The Kinabalu granite was intruded, under extensional

stress, into the central Crocker Mountains in the Late Miocene (7-8 Ma; Cottam *et al.*, 2010; Burton-Johnson *et al.*, 2017, 2019). The nearest contemporaneous granitic magmatism is the Capoas Granite (Fig. 1a), 600 km to the NE in Palawan (13.5 Ma, Suggate *et al.* 2013), although <5 Ma enriched basaltic to dacitic magmatism is recorded in Borneo on the Semporna Peninsula, and at Usun Apau and Linau Balui (Fig. 1a, Macpherson *et al.*, 2010; Cullen *et al.*, 2013).

Field relations of the Mt Kinabalu pluton

The Mt Kinabalu pluton was emplaced as six major granitic units (Fig. 1c, see Burton-Johnson *et al.*, 2017 for petrographic descriptions). Revised field relationships and U-Pb zircon ages have shown that the composite pluton was initially emplaced from the top down in a broadly laccolithic structure through upward deformation of the host rocks (Cottam *et al.*, 2010; Burton-Johnson *et al.*, 2017). Consequently, the oldest unit, the Alexandra Tonalite/Granodiorite (7.85 ±0.08 Ma), lies above subsequent, larger units of the Low's Granite (7.69 ±0.07 Ma) and the King Granite (7.46 ±0.08 Ma). The smaller, vertical, planar Donkey Granite (7.49 ±0.03 Ma) intruded the King Granite before the latter could fully crystallise, producing contacts that vary between gradational and mingled. The final two porphyritic units (the Paka Porphyritic Granite, 7.32 ±0.09 Ma, and the Mesilau Porphyritic Granite, 7.22 ±0.07 Ma) deviate from the laccolith model having been emplaced laterally and around the periphery of the earlier units (Fig. 1c; Burton-Johnson *et al.*, 2017). Field evidence for the approximate volumes of the pluton's composite units (Fig. 1c, Burton-Johnson *et al.*, 2017) and the U-Pb zircon ages (Cottam *et al.*, 2010) give a total pluton volume of ~170 km^3 and a total emplacement period of 0.6 Myr. This equates to an average

emplacement rate of ~3 x10^{-4} km^3yr^{-1}; comparable with evidence from other plutons worldwide (de Saint Blanquat *et al.*, 2011; Menand *et al.*, 2015).

METHODOLOGY

Samples were analysed from each granitic unit, from the turbidite overburden of the Crocker Formation, and from a xenolith found in the intrusion (a conglomerate within the Donkey Granite, Fig. 1). Samples were powdered by fly press and agate ball mill.

Major element chemistry was obtained by XRF at Edinburgh University. Samples were dried at 1100°C, mixed with $LiBO_2$ flux and fused into glass discs for analysis (Gill, 1997). Trace element chemistry was obtained on a ThermoScientific X-Series 2 ICP-MS (Durham University). The methodology, blank, and detection limits are given in Ottley *et al.* (2003). Sample powders were dissolved using HF and HNO_3, and blanks, repeated samples and the standards BHVO-1, W2 and AGV-1 analysed for calibration and quality control (Ottley *et al.,* 2003). To ensure zircon dissolution, granitic samples were fused prior to crushing and dissolution. Accuracy and reproducibility were monitored using standards AGV-1, BHVO-1, and W2, and through replicate analyses of Mt Kinabalu samples (Supplementary Data 1 and Burton-Johnson, 2013).

Radiogenic isotope compositions were obtained by Plasma Ionisation Multi-collector Mass Spectrometer (PIMMS, Durham University). Sr and Nd isotopic analyses followed the column chemistry procedures of Charlier *et al.* (2006). Whole-rock powders were dissolved in HF and HNO_3 SpA acid and separated by column chemistry using Sr-spec resin and Hf-Nd cation resin (AG50 X-8). The lead fraction was collected in 100µl 8N HCl from the Sr columns following collection of the Nd

and Sr fractions and elution of waste using 200µl 2.5N HCl. The Pb fraction was dried down, dissolved in 500µl 3% HNO_3, and spiked with ^{206}Tl to correct for mass bias (Hirata, 1996). PIMMS analytical procedures are detailed in Nowell *et al.* (2003). For Nd and Sr, measured values for the NBS987 and J&M standards (±2SD error) during the same run as the samples were 0.710269 ±23 (n=35) and 0.511110 ±11 (n=44) respectively. Data are corrected to the respective NBS987 and J&M standard values of 0.71024 (Thirlwall, 1991) and 0.511110 (Royse *et al.,* 1998). For Pb, measured values for the NBS981 standards ±2SD for $^{206}Pb/^{204}Pb$, $^{207}Pb/^{204}Pb$, $^{208}Pb/^{204}Pb$, $^{207}Pb/^{206}Pb$ and $^{208}Pb/^{206}Pb$ (n=20) are 16.9405 ±9, 15.4981 ±9, 36.7177 ±23, 0.91486 ±3 and 2.1674 ±1 respectively. Data are corrected to the respective values of NBS981 of 16.9405, 15.4980, 36.7174, 0.91485 and 2.1674 (Galer, 1997).

Oxygen isotope ratios of mineral separates were analysed by laser fluorination (SUERC, East Kilbride). Oxygen was extracted by heating c. 1mg of sample with a laser in the presence of ClF_3 (Mattey & Macpherson, 1993). Oxygen was converted to CO_2 and isotopic ratios were analysed using a VG PRISM 3 dual inlet mass spectrometer. Results are reported as $\delta^{18}O$ values in per mil (‰) deviations from Vienna Standard Mean Ocean Water (V-SMOW). For precision, all sample analyses were repeated. Four analyses of the reference standards SES, GP147 and UWG2 were made each day for daily calibration, and their mean daily standard error from published isotopic values is 0.15‰; the maximum daily standard error was 0.26%.

Major element mineral chemistry was determined for polished thin sections using a JEOL JXA-8100 Superprobe electron microprobe (EMP) paired with an Oxford Instruments INCA energy-dispersive microanalytical system (EDS) at Birkbeck College. Analyses were performed using an accelerating voltage of 15 kV, a beam current of 10 nA, and a beam diameter of 1 µm. Calibration used standards of

natural silicates, oxides, and Specpure metals, and a ZAF correction procedure was applied. XFe^{3+} (Fe^{3+}/Fe_{total}) for individual minerals was calculated from the charge balance and stoichiometry.

RESULTS

Data for all whole-rock major and trace element geochemical analyses are presented in Table 1, and whole-rock isotope data and mineral separate oxygen isotope data in Table 2. Major element mineral chemistry is reported in Supplementary Data 2.

Major and trace elements

Mineralogically the individual units that comprise the Mt Kinabalu intrusion are largely granites (Burton-Johnson *et al.,* 2017). Geochemically the Alexandra Tonalite/Granodiorite and Low's Granite are diorites, whereas later units are granodiorites and syenodiorites (Fig. 2a). Our analyses show a similar range in compositions to previous analyses by Vogt & Flower (1989), but coupling geochemical data with mapping (Burton-Johnson *et al.,* 2017) and geochronological data (Cottam *et al.,* 2010) allows us to recognise a more refined structure of units (Fig. 2). All units are sub-alkalic and enriched in potassium, with the Alexandra Tonalite/Granodiorite and Low's Granite classified as high-K calc-alkaline, and the later units as shoshonitic (Fig. 2b). While the Alexandra Tonalite/Granodiorite is weakly peraluminous, all subsequent units are metaluminous. Amphibole chemistry is calcic and dominantly magnesio-hornblende in classification (Fig. 3).

Trace element ratios show that the Kinabalu rocks display uniform, relative depletion in Nb and Ta, and enrichment of K and Pb. Such signatures are similar to

those of continental crust or arc magmas. Chondrite-normalised REE plots (Fig. 4) show elevated LREE/HREE and concave middle to heavy REE. Each unit displays a negative Eu anomaly.

Radiogenic Isotopes

The Alexandra Tonalite/Granodiorite ($^{87}Sr/^{86}Sr_i$ ~0.7076; $^{143}Nd/^{144}Nd_i$ ~0.51247 (εNd -3.19); $^{206}Pb/^{204}Pb_i$ ~18.754) is consistently displaced farther from mantle compositions than the younger intrusive units ($^{87}Sr/^{86}Sr_i$ ~0.7066, $^{143}Nd/^{144}Nd_i$ ~0.51251 (εNd -2.39) and $^{206}Pb/^{204}Pb_i$ ~18.724). Likewise, the Mt Kinabalu isotope compositions are displaced to more radiogenic Sr and Pb, and less radiogenic Nd than uncontaminated, mantle-derived basalts from Borneo and the adjacent South China Sea (Fig. 5a, Chen *et al.*, 2008; Wang *et al.*, 2008; Macpherson *et al.*, 2010; Cullen *et al.*, 2013). Isotopically, the Kinabalu rocks (Fig. 5) are more similar to Mesozoic granites from the South China Sea (Yan & Shi, 2009; Yan *et al.*, 2010), the Capoas granite of Palawan (Encarnación & Mukasa, 1997; Burton-Johnson, 2013), and the least radiogenic rocks from Vietnam, Hong Kong and Yunnan (Thuy *et al.*, 2004). Pb data for the regional magmatism, including Mt Kinabalu, diverges from the Northern Hemisphere Reference Line (NHRL) towards an enriched mantle (EMII) composition (Fig. 5b, Zindler & Hart, 1986), as noted by previous authors (Hoang *et al.*, 1996; Yan *et al.*, 2008).

Oxygen Isotopes

$\delta^{18}O$ values range between +9.4 and +10.3‰ for quartz, and between +6.6 and +8.2‰ for hornblende (Fig. 6). By analysing both hornblende and quartz, post-crystallisation

alteration of the oxygen isotope composition can be assessed. Equilibration at magmatic temperatures produces lower and more restricted $\Delta^{18}O_{quartz\text{-}hornblende}$ isotope values (where $\Delta^{18}O_{quartz\text{-}hornblende} = \delta^{18}O_{quartz} - \delta^{18}O_{hornblende}$) than lower temperature equilibration with altering fluids. Measured $\Delta_{quartz\text{-}hornblende}$ values are equivalent to temperatures of 650-1100°C (Fig. 6; Lackey *et al.*, 2008, and references therein). Within error (Fig. 6), this range is reasonable for mineral-mineral equilibrium in felsic magmas containing hornblende, which, at 200 MPa vapour-saturated conditions, should be stable below 960°C (±10°C) to a solidus temperature of 675° (±25°C, Naney, 1983).

Assuming that $\delta^{18}O$ values of all minerals represent magmatic conditions, we can estimate magmatic $\delta^{18}O$ values for all the other minerals by employing $\Delta_{mineral\text{-}hornblende}$ values (Lackey *et al.*, 2008, and references therein) for the temperatures determined by $\Delta_{quartz\text{-}hornblende}$ thermometry. A $\delta^{18}O$ for the bulk magma from which each sample crystallised can then be calculated through mass balance using: (1) the estimated magmatic $\delta^{18}O$ of each phase, and (2) the modal proportions of each phase in each sample (as measured by point-counting, Burton-Johnson *et al.*, 2017). We used this methodology for determining whole-rock $\delta^{18}O$ in preference to bulk sample analysis of $\delta^{18}O$ due to the slow diffusion rate of oxygen in hornblende (Farver & Giletti, 1985). This method thus allows an estimate of magmatic $\delta^{18}O$ without the influence of meteoric water alteration, which would otherwise result in sub-solidus $\delta^{18}O$ alteration of phases possessing a faster diffusion rate (e.g. quartz and feldspar).

DISCUSSION

The only previous geochemical study of Mt Kinabalu (Vogt & Flower, 1989) concluded that rocks of the Alexandra Tonalite/Granodiorite unit (then termed the Biotite Quartz Monzodiorite by Vogt & Flower, 1989), represented the most primitive magma in the intrusion and were produced by re-melting of underplated basalt. It was proposed that all other units (collectively referred to as Hornblende Quartz Monzonite) were the result of further crustal contamination of the Biotite Quartz Monzodiorite. Our isotopic data demonstrate that the Alexandra unit has the most "crustal" isotopic ratios and so this relationship with the rest of the intrusion is unlikely. Furthermore, the model developed by Vogt & Flower (1989) assumed that the Alexandra unit was at the core of a nested diapir and so represented the youngest unit of Kinabalu. Mapping and U-Pb geochronology of zircon has subsequently demonstrated that the intrusion is layered with the Alexandra unit being its oldest component (Fig. 1; Cottam *et al*., 2010).

Granitic melts can be derived through fractionation of mantle-derived melts, with or without crustal assimilation (assimilation and fractional crystallisation, AFC), or through partial melting of crustal lithologies (crustal anatexis) (e.g. Bogaerts *et al.*, 2006; Jagoutz *et al.*, 2009; Clemens & Benn, 2010; Chappell & White, 2011; Leuthold *et al.*, 2012; Jagoutz & Klein, 2018). We combine our new geochemical data with mapping and geochronological constraints to evaluate the likelihood that the Mt Kinabalu magma was generated by these three mechanisms.

Crustal anatexis

Potential crustal sources for the Mt Kinabalu magma are: (i) ophiolitic basement; (ii) turbidite sediments; (iii) older felsic continental crust beneath Sabah (previously

postulated by Macpherson *et al.* 2010); (iv) continental crust underthrust beneath Borneo during the final stages of Proto South China Sea subduction; or (v) gabbroic lower crust (Vogt & Flower, 1989). The isotopic ratios of Mt Kinabalu rocks are sufficiently displaced from mantle compositions for us to discount an origin solely from melting ophiolitic basement. However, the radiogenic isotopes cannot conclusively rule out the other possibilities, particularly as the turbidite sediments are variable in their composition, while the monzogranites and tonalites dredged from attenuated continental crust of the South China Sea share similar isotopic signatures to Mt Kinabalu (Fig. 5).

To evaluate the feasibility of producing Mt Kinabalu magma by crustal anatexis, we compiled data for melting experiments on igneous and sedimentary rocks and their metamorphic equivalents (Fig. 7). These experiments were conducted on a wide range of compositions over a range of temperatures, pressures, water contents and redox conditions. The alkali metal compositions show that the different protoliths produce melts with distinctive compositional ranges, regardless of the degree of melting (Fig. 7). Melting of a sedimentary protolith generates peraluminous melt compositions with high K/Na and very low Ca/Na ratios, and with very restricted ratios of Al/(Na+ K): Al/(Ca + Na + K) (Fig. 7). Melting felsic crustal protoliths yields similar compositions, but these tend to have even higher and more scattered K/Na (Fig. 7a). None of these protoliths generates comparable melts to the largely metaluminous, high-Ca/Na and high K/Na samples from Mt Kinabalu.

Partial melts of basaltic lithologies range from peraluminous to metaluminous (~90% are peraluminous) and their Al/(Na+ K): Al/(Ca + Na + K) ratios can resemble those of Kinabalu rocks (Fig. 7b). However, their generally low K/Na ratios and consistently low Ca/Na ratios (Fig. 7a) suggest that these are also unlikely sources for

the Kinabalu magmas. This corroborates our earlier inference made on the basis of isotopic ratios. Only melts derived from exceptionally Ca-rich and Na- and K-deficient basaltic amphibolites (Wolf & Wyllie, 1994) possess Ca/Na ratios as high as Kinabalu (Fig. 7a), but these are strongly peraluminous with exceptionally high Al/(Na + K), and K/Na much lower than the Mt Kinabalu granitoids. This also means that any mixture of such high Ca/Na melt with high K/Na sources would remain peraluminous, dissimilar to Mt Kinabalu. Consequently, melts derived solely from crustal anatexis, be they from a single source or any likely mixtures (including the mafic lower crust), cannot reproduce the major element composition of Mt Kinabalu, or other metaluminous and intermediate to high Ca/Na and K/Na magmatism.

Prouteau *et al.* (2001) suggested that the Kinabalu intrusion is adakitic. We dispute an origin for the Mt Kinabalu magma through melting of subducted oceanic crust as the major element compositions of partial melts from hydrous, basaltic amphibolites (Winther & Newton, 1991; Sen & Dunn, 1994; Rapp & Watson, 1995) are distinct from the Kinabalu rocks (Fig. 7). Neither our data, nor that from preceding studies (Vogt & Flower, 1989), possess the distinctive trace element signatures of these putative slab melts (Defant & Drummond, 1990). Furthermore, the radiogenic isotope ratios of all Kinabalu units lie outside the fields of most ocean floor basalts, including the South China Sea (Fig. 4). Therefore, we dismiss this as a possible origin for the Kinabalu magmas.

Fractional crystallisation of mantle-derived basalt

Experimental petrology demonstrates the potential for fractional crystallisation of mafic magmas to produce granitic melts (e.g. Grove *et al.*, 2003; Alonso-Perez *et al.*, 2009; Nandedkar *et al.*, 2014; Müntener & Ulmer, 2018). There is no evidence in

the immediate vicinity of Mt. Kinabalu for contemporaneous mafic magmatism, but Neogene basaltic volcanism occurred in other north Borneo locations, such as Semporna, Usun Apau and Linau Balui (Fig. 1a, Macpherson *et al.,* 2010; Cullen *et al.,* 2013), with evidence of differentiation to more felsic compositions at these locations. However, fractional crystallisation alone cannot be responsible for the range of Kinabalu magma compositions. The isotope ratios of Sr, Nd and Pb are all substantially displaced from those of Neogene basalts from Borneo, other than those identified as having experience substantial crustal contamination (Fig. 5; Macpherson *et al*., 2010). There is also significant variation between the different Kinabalu units, without large contrasts in trace element ratios, which are more readily reconciled with open-system behaviour in the crust. This is further suggested by the large range of oxygen isotope ratios, which include values for mafic phases, such as hornblende, that are substantially higher than those that would be expected to be in equilibrium with mantle-derived magma (Mattey *et al.,* 1994; Macpherson & Mattey, 1998; Lackey *et al.,* 2008). Therefore, we conclude that the isotopic diversity of the Mt Kinabalu granitic intrusion cannot be explained by the fractionation of mantle-derived basalt alone, and instead requires open-system processes in the Borneo crust.

Crustal contamination of magma: Equilibrated Major Element – Assimilation with Fractional Crystallisation (EME-AFC)

To model open-system behaviour for the various geochemical properties considered here we developed an incremental major element AFC model termed Equilibrated Major Element AFC (EME-AFC). This was undertaken because the thermodynamic model MELTS (Ghiorso & Sack, 1995) is not recommended for felsic or intermediate systems, and neither MELTS nor rhyolite-MELTS (which can model high-silica

systems, Gualda *et al.*, 2012) can model hydrous magmatic systems involving substantial hornblende or biotite fractionation. The Magma Chamber Simulator (Bohrson *et al.*, 2014) utilises Rhyolite-MELTS, so is also unable to model systems involving significant fractionation of hydrous phases. Additionally, mass balance equations do not reflect the changing compositions of mineral phases in response to the geochemical evolution of the magma. Instead we developed EME-AFC modelling, which employs two-component major element partition coefficients ($K_D^{X,Y}=(X^{Min}.Y^{Liq})/(Y^{Min}.X^{Liq})$), where X and Y are elements in a single mineral phase (^{Min}) in equilibrium with a liquid (^{Liq}). This allows simultaneous modelling of major elements by EME-AFC, and trace elements, radiogenic isotopes, and oxygen isotopes by recognised methods (DePaolo, 1981).

The major element component of EME-AFC is similar to that of Grove & Donnelly-Nolan (1986) in which the Fe-Mg and Ca-Na compositions of the fractionating phases equilibrate with the evolving magma. This involved calculating the Fe-Mg and Ca-Na phase compositions using two-component major element partition coefficients ($K_D^{Fe,Mg}=(Fe^{Min}.Mg^{Liq})/(Mg^{Min}.Fe^{Liq})$ and $K_D^{Ca,Na}=(Ca^{Min}.Na^{Liq})/(Na^{Min}.Ca^{Liq})$) and solving for successive increments of fractionation (F). We broadened this approach to a larger number of phases, equilibrating more elements and calculating the concentrations of all major and minor elements in each phase. Assimilation is modelled at each increment by binary mixing for the major elements according to a user-determined rate, r (the mass assimilated / mass crystallised), which is the parameter in AFC modelling describing the ability of magma to assimilate crust (DePaolo, 1981; Reiners *et al.*, 1995). The formulae for each phase and the sites into which elements can substitute are determined from Deer *et al.* (1992) and the valency of each element. The Fe-Mg, Al-Si and K-Na partition

coefficients (Table 3) are determined from experimental data (Grove *et al.*, 2003; Alonso-Perez *et al.*, 2009; Nandedkar *et al.*, 2014). Note that, unlike trace element partition coefficients (Supplementary Data 6), two-component major element partition coefficients have narrow ranges of values (Table 3). Consequently, as in the "Crustal anatexis" section, our subsequent discussion of the EME-AFC modelling focuses on the major elements.

Plagioclase fractionates as $((K,Na)_{1-(x-1)},(Mg+Mn+Ca)_{x-1})_1((Fe+Al)_x,Si_{4-x})_4O_8$ and its equilibrium with the coexisting evolving liquid is determined by the two-component distribution coefficient $K_D^{Al,Si} = Al^{Plag}Si^{Liq}/Si^{Plag}Al^{Liq}$. The Al-Si distribution is used in preference to the Ca-Na distribution as $K_D^{Al,Si}$ in plagioclase is far less variable than $K_D^{Ca,Na}$ (1.8-4.2, compared to 0.6-16.2, Grove *et al.*, 2003; Alonso-Perez *et al.*, 2009; Nandedkar *et al.*, 2014). The Na-K distribution is calculated from $K_D^{K,Na} = K^{Plag}Na^{Liq}/Na^{Plag}K^{Liq}$. Fe substitutes for Al, and Mg, and Mn substitute for Ca in proportions determined empirically from the Mt Kinabalu mineral chemistry (Supplementary Data 3). Hornblende fractionates as $(Na,K)_{0-1}Ca_2((Mn,(Mg,Fe)),(Ti(Al,Si)))_{13}O_{22}(OH)$, and its equilibrium with silicate liquid is determined using the Fe-Mg and Al-Si two-component partition coefficients: $K_D^{Fe,Mg} = Fe^{Hb}Mg^{Liq}/Mg^{Hb}Fe^{Liq}$ and $K_D^{Al,Si} = Al^{Hb}Si^{Liq}/Si^{Hb}Al^{Liq}$. Orthopyroxene and clinopyroxene fractionate as $((Ca,Na),(Mn,(Mg,Fe)))_2(Si,(Ti,Al))_2O_6$ and use the Fe-Mg and Al-Si mineral-melt distribution coefficients: $K_D^{Fe,Mg} = Fe^{Opx}Mg^{Liq}/Mg^{Opx}Fe^{Liq}$, and $K_D^{Al,Si} = Al^{Cpx}Si^{Liq}/Si^{Cpx}Al^{Liq}$. Biotite fractionates as $(K,Na)_2((((Mg,Fe)Ti)Mn)_{4-6},(Al,Si)_{8-10})_{14}O_{20}(OH)_4$, and equilibrates with the liquid using $K_D^{Al,Si} = Al^{Plag}Si^{Liq}/Si^{Plag}Al^{Liq}$. Both olivine and garnet equilibrate using Fe-Mg mineral-melt partition coefficients and fractionate as $((Mg,Fe),Ca,Mn)_2(Si,Al,Ti)O_4$, and $(Mg,Fe)_3Al_2\ Si_3O_{12}$, respectively. Major and minor element concentrations not

determined by two-component partition coefficients or stoichiometry are calculated for each phase by mean or linear regression correlations with other major elements in the mineral separate data (Supplementary Data 3). These calculations along with a detailed explanation of the major element modelling are presented in Supplementary Data 3 and Supplementary Data 4, as well as the EME-AFC modelling spreadsheet (Supplementary Data 5).

The trace element and isotopic components of EME-AFC are calculated at each increment using the AFC equations of DePaolo (1981). Trace element partition coefficients are compiled and calculated from the GERM database (https://earthref.org/KDD/), except for quartz (Nash & Crecraft, 1985). Where reasonable, absent REE partition coefficients are interpolated. The compiled and calculated partition coefficients and their references are provided in Supplementary Data 6. Partial melting of the assimilant prior to assimilation in the melt is incorporated for the trace elements by modal batch melting with user-determined assimilant mineralogy and melt fraction ($F_{\text{Assimilant}}$).

To accommodate the changing nature of element partitioning during magmatic differentiation, EME-AFC employs four intervals of SiO_2 content representing melt compositions of basalt, basaltic andesite, andesite and rhyolite (note that the basaltic andesite starting material for the Mt Kinabalu models below is more evolved than the basaltic interval). Each interval uses appropriate major and trace element partition coefficients (Table 3). The two-component major element partition coefficients used in the EME-AFC model do not correlate with melt SiO_2 except for the Al-Si coefficient of plagioclase, which changes in the model at 57 and 63 wt % SiO_2. In addition to the magmatic composition, at each increment the composition of the bulk cumulate assemblage, the total fraction of melt remaining in the system, and the total

ratio of the mass of assimilated material to the initial magma mass (ρ) are calculated. To constrain the fit of the model through trial and error, the sum of the differences squared (ΣD^2) for the major elements of the model and target composition is also calculated.

Oxygen isotope fractionation between coexisting phases varies with temperature. Multivariate linear regression of experimental fractionation data for experimental conditions of 700-1300°C, 0-11% H_2O and 7-12 kbar, shows that melt SiO_2 contents correlate strongly with temperature (Fig. 8), moderately with H_2O, but do not correlate with pressure (respective p-values of $6x10^{-13}$, 0.02 and 0.7). Thus, we derived an empirical relationship between SiO_2 and temperature ($T=-19SiO_2+2050$, $R^2 = 0.75$, ±62°C at 1SD). This allows the temperature, resultant $\Delta_{Mineral-Melt}$, $\delta^{18}O$ of the fractionating assemblage, and $\delta^{18}O$ of the magma to be calculated at each model increment.

Each potential fractionating phase has specific effects on the major element, trace element, and isotopic composition of the evolving melt. This means that, in comparison with modelling geochemical properties in isolation, EME-AFC greatly limits the range of possible fractionating assemblages that can generate a target composition.

EME-AFC has specific advantages over existing AFC models: the ability to model felsic systems and those dominated by the fractionation of hydrous mineral phases (biotite and hornblende); simultaneous modelling of major and trace elements, and radiogenic and stable isotopes; control of the fractionating system and its parameters allows exploration of each parameter or input's effects on the liquid line of descent; and, importantly, the effects of pressure, water content and oxidation state

of the system are accounted for by calibrating the model to the specific mineral chemistry of the system under consideration. In addition, the EME-AFC model is run within a standard spreadsheet, without the requirement for specialist software or specific operating systems.

Evaluation of EME-AFC modelling

EME-AFC modelling was developed to address the absence of AFC modelling solutions for felsic systems involving substantial amphibole or biotite fractionation. To validate this approach we compared the outputs of EME-AFC with those of Rhyolite-MELTS (Gualda *et al.*, 2012) for fractional crystallisation models of two discrete starting compositions: a Mid-Ocean Ridge Basalt (Allan *et al.*, 1989) and a basalt from Borneo (Macpherson *et al.*, 2010).

The detailed comparison (Supplementary Data 7) shows that EME-AFC broadly reproduces the liquid lines of descent (LLD) calculated by Rhyolite-MELTS (Fig. 9). For both starting compositions the largest discrepancy results from Rhyolite-MELTS fractionating high-Al clinopyroxene (>13.5 wt % Al_2O_3) below 1075°C. Due to the relationship of Al and Si in the fractionating phase compositions (Table 3), this affects Si as well as Al evolution. Consequently, remaining melt fractions are smaller in the Rhyolite-MELTS models for the same SiO_2 concentration in EME-AFC. This also influences the apparent LLD for all major elements compared with SiO_2. However, neither suite shows evidence for the presence of high-Al pyroxene (Allan *et al.*, 1989). Pyroxenes in mafic lavas are expected to contain Al_2O_3 concentrations <9 wt %, and even lower concentrations are expected for metaluminous or MORB basalts similar to those modelled (Le Bas, 1962; Nisbet & Pearce, 1977). Thus, the suitability of the calculated Rhyolite-MELTS fractionating assemblage is ambiguous,

whilst the EME-AFC clinopyroxene Al_2O_3 compositions more similar to the expected mineral chemistries of the settings modelled (Le Bas, 1962; Nisbet & Pearce, 1977).

EME-AFC modelling of Mt Kinabalu

A Linau Balui basaltic andesite sample (LB85, Cullen *et al.*, 2013) was chosen as the initial melt. This is the most local basalt for which a comprehensive major element, trace element, and radiogenic isotope dataset was available. The $\delta^{18}O$ value of LB85 is not known, but the primary melts can be assumed to have a value of +5.5‰ due to the limited variation of magmas derived from the mantle (5.5 ±0.35‰, Mattey *et al.*, 1994; Macpherson & Mattey, 1998). Metasedimentary xenoliths are the only recorded field evidence for crustal assimilation at Mt Kinabalu (Vogt & Flower, 1989; Burton-Johnson, 2013). Thus a constant elemental and isotopic composition from a metamorphosed conglomerate xenolith found within the Donkey Granite (Fig. 5) was used as the assimilant in the initial models.

Applying the model to the most voluminous unit of Mt Kinabalu, the King Granite, most of the mineral chemistries (Fig. 10) and chemical variation of the pluton can be generated through EME-AFC modelling with the exception of K and Na. Regardless of the fractionating assemblage and degree of assimilation, the high-K chemistry of Mt Kinabalu cannot be replicated by assimilation of the meta-conglomerate xenolith (Fig. 11, Model 1). Experimental petrology has shown that partial melts of metasediments develop higher K than their protoliths (Fig. 7, Le Breton & Thompson, 1988; Vielzeuf & Holloway, 1988; Douce & Johnston, 1991; Gardien *et al.*, 1995; Montel & Vielzeuf, 1997). From these studies, the biotite, plagioclase, and quartz (BPQ) starting material for the melting experiments of Gardien *et al.* (1995) most closely resembles the mineralogy and chemistry of the

meta-conglomerate. Incorporating this melt composition into the EME-AFC model replicates the sense of K-enrichment required for the Alexandra unit (Fig. 11a, Model 2). However, the higher K-enrichment of the majority of units at Mt Kinabalu cannot be reproduced by this assimilant chemistry (Fig. 11a, Model 2) and the Na compositions of the Mt Kinabalu intrusive rocks are poorly reproduced (Fig. 11b, Model 2).

Increasing the modelled K_2O concentration of the BPQ assimilant further shows that the K_2O composition of Mt Kinabalu requires the assimilant to contain up to 12 wt % K_2O. Despite the range of protolith compositions, degrees of melting, and melting conditions in the compiled data for melting experiments (as used in Fig. 7), the highest K_2O concentration in the partial melt was 7.7 wt % from a metapelite (Douce & Johnston, 1991). Consequently, it is unlikely that the K-enrichment of Mt Kinabalu results from assimilation alone.

Instead, the simplest resolution to the offset from observed alkali contents is to postulate a wider range of precursor K-contents in the initial melts. A potential, contemporaneous analogue for such heterogeneity can be found in central Borneo. At 8 Ma, coincident with the formation of the Mt Kinabalu intrusion, minette dykes were emplaced at Linhaisai (Fig. 1a) as a result of low-degree melting of a metasomatised, fertile mantle source (Bergman *et al*., 1988). These have K_2O contents ranging from 2.15 to 6.30 wt % in relatively low silica melts (Fig. 11a). These same minettes also have relatively low Na contents compared to Neogene basalts from Borneo (Fig. 11b). It is unlikely that the volume of magma, or the heat to generate substantial crustal melting at Kinabalu, could be produced from a phase of minette-style magmatism. However, the occurrence of contemporaneous high-K, low-Na magmatism suggests that the mantle beneath Borneo may exhibit substantial enrichment that could

generate mafic precursors of a composition between that of minette and the mafic, intraplate magma inferred for Semporna and Linau Balui (Macpherson *et al*., 2010; Cullen *et al*., 2013). Increasing the primary magma K_2O to 2.5 wt % and reducing the primary magmatic Na_2O to 2.1 wt % generates metaluminous melts with alkali metal compositions similar to Mt Kinabalu (Fig. 11b and 11c, Model 3).

The range of the King Granite compositions (including major and trace elements, and isotopes) can be modelled by contamination of the modified primary melt (2.1 wt % Na_2O, 2.5 wt % K_2O) by a partial melt of the meta-conglomerate. In the absence of partial melt data for the meta-conglomerate xenolith, this was simulated using the major element composition of the BPQ partial melt used in Model 2 (Fig. 11, Gardien *et al*., 1995) and the analysed trace elements of the xenolith, modelled to the same degree of partial melting as the BPQ melting experiment ($F_{\text{Assimilant}} = 0.09$).

The King Granite compositions are generated through the bulk cumulate fractionation of: 42-47% plagioclase, 14-17% clinopyroxene, 14-17% orthopyroxene, 18-20% hornblende, 0.5% apatite, 1.5% magnetite, 3.5% ilmenite, and 0.01% zircon (Fig. 12; Table 4). A $\delta^{18}O$ value of +10‰ is required for the assimilant, which is a suitable value for this siliclastic sedimentary lithology (Magaritz *et al.,* 1978). The degree of fractionation, F (the fraction of melt remaining) is 0.54-0.66, while the required assimilation rate, r (mass assimilated / the mass crystallised at each increment of F) is 0.4-0.57, resulting in a value for ρ (the total ratio of the mass of assimilated material to the initial magma mass) of 0.23-0.25.

Although energy constrained AFC modelling (EC-AFC, Spera & Bohrson 2001) is unable to model major elements, it can be used to determine thermodynamic constraints for our model. EC-AFC indicates that r values of 0.4-0.8 are reasonable

for our system, given the proposed input chemistries, pre-emplacement assimilation at mid-crustal depths, and temperatures of basaltic magma. Thermodynamic modelling of AFC processes has shown that *r* is variable during magmatic evolution (Reiners *et al.*, 1995) and, thus, the EME-AFC model (Supplementary Data 5) can accommodate variable *r*. However, in the interest of not overcomplicating the Mt Kinabalu models, and presenting the EME-AFC methodology here for the first time, *r* is treated as a constant in this scenario.

Modelling the compositions of the remaining units indicates that similar conditions could produce the other units. However, slight differences in chemistry indicate the broad evolution of the intrusion through its emplacement. The compositional range of the Donkey Granite, Paka Porphyritic Granite and Mesilau Porphyritic Granite are similar to the King Granite (Fig. 12) so can be replicated by similar EME-AFC parameters, but with variations in the degree of fractionation (F = 0.5-0.74), r (0.36-0.66), and ρ (0.2-0.25). This is more marked for the less evolved compositional range of the earlier Low's Granite, which reflects significantly lower degrees of fractionation (F = 0.72-0.78). Despite this, the isotopic ratios of the Low's Granite are similar to those of the more evolved units, suggesting a higher assimilation rate (r = 0.65-0.73, ρ =0.16-0.21). Likewise, a similar fractionating assemblage can also produce the compositional range of the earliest unit, the Alexandra Tonalite/Granodiorite (F = 0.59-0.73), but also requires a high rate of assimilation (r = 0.56-0.72, ρ =0.22-0.29) and either no K-enrichment of the primary magma or more complete melting of the assimilant (Fig. 10a). Alexandra also requires a higher $^{207}Pb/^{204}Pb$ ratio in the assimilant than other units (Fig. 12), indicating isotopic heterogeneity in the assimilant. The assimilation rate, *r*, in these two oldest units is higher than those that follow, but within the range of values predicted by EC-

AFC. The subsequent decrease in *r* may reflect the reduced fertility of the assimilant following early intrusive episodes. As the source, assimilant, and fractionating assemblages are similar for all units, this reduction in assimilation rate and the degree of fractionation may have been the primary cause of geochemical heterogeneity in the Mt Kinabalu intrusion.

Due to the pluton's exceptional vertical exposure, the contacts and composite unit volumes can be constrained (Fig. 1, Burton-Johnson *et al.*, 2017). Combining this with the outputs from the EME-AFC model allows us to estimate the volume of mantle-derived magma emplaced into the crust and the volume of crust assimilated. The total pluton volume (V_p) can be expressed as:

$$V_p = V_0 - V_c + V_a$$

[Eq. 1]

Where V_0 is the primary magma volume, V_c is the volume of fractionated material and V_a is the volume of assimilated anatectic melt from the crust. If V_c = (1-*F*) and $\rho = V_a/V_o$ then:

$$V_0 = (V_p + 1 - F)/(\rho + 1)$$

[Eq. 2]

Allowing a conservative 20% error in the volume estimation of the composite units, the 140-210 km^3 total pluton volume can be generated by 115-176 km^3 of primary magma and 25-43 km^3 of assimilated crust.

Nature of the crustal contaminant

As shown by EME-AFC modelling, partial melts of the conglomerate xenolith are a suitable analogue for the crustal contaminant required to generate the chemical heterogeneity of intrusive units at Mt Kinabalu. Further insight into the nature of the contaminating crust can be gained by comparing the inherited zircon population of Mt Kinabalu (Cottam *et al.,* 2010) to the detrital zircon populations of the regional sedimentary units (Fig. 13; van Hattum *et al.,* 2013). The Mt Kinabalu zircon population has a prominent inherited population with ages of 96 to 147 Ma, with rare, older Mesozoic ages and very few Palaeozoic or Precambrian Ages (Fig. 13). This contrasts with zircon populations hosted in the region's deep-water turbidite deposits of the Oligocene units of the Crocker Formation and the Eocene Sapulut and Trusmadi Formations, each of which have a substantial population of early Mesozoic and Palaeozoic zircons, with or without notable Precambrian peaks (Fig. 13). The Upper Eocene unit of the Crocker Formation displays a very similar distribution of inherited zircon ages to Mt Kinabalu (Fig. 13) and, therefore, represents the most likely local, siliclastic source of the xenoliths and the contaminant of the magma that constructed the pluton.

Origin of the magmatism

Mt Kinabalu is isolated from any contemporaneous mafic or felsic magmatism. Intraplate basalts and andesites from the Semporna peninsula (Fig. 1a) are the closest occurrence of magmatism but are younger than Kinabalu and appear to have been generated under lithosphere that was previously thinned by subduction between the Celebes and Sulu Seas (Macpherson *et al.,* 2010). The Semporna magmatism may also be associated with other younger sites in central, northern Borneo, such as Usun

Apau and Linau Balui (Cullen *et al.*, 2013), and possibly as far afield as Niut in western Borneo (Harahap, 1994); however, the difference in ages of these events suggests there is no direct link with Mt. Kinabalu.

The only contemporaneous magmatism on the island is the Linhaisai minette in central Borneo (Fig. 1a) for which K-Ar dating of phlogopite (7.8 ±0.3 Ma, Bergman *et al.*, 1988) gives almost identical ages to U-Pb dating of Kinabalu zircon (7.22-7.85 Ma, Cottam *et al.*, 2010). As discussed above, the large distance between these suggest it is unlikely that they are part of the same magmatic system. However, the emplacement of two magmatic bodies, each requiring an input of primitive magma from an enriched mantle source, suggests that regional controls on mantle melting may have operated at this time.

Structural and Anisotropic Magnetic Susceptibility data (Burton-Johnson *et al.*, 2019) indicate that Mt Kinabalu was emplaced into a zone of NNW-SSE extension, possibly the result of SE-directed slab rollback during Celebes Sea subduction to the SE (Cottam *et al.*, 2013; Hall, 2013). Extension of the crust may have provided pathways through which relatively low-degree partial melts from enriched mantle could intrude and heat the crust, allowing generation of a body composed of both mantle and crustal melts. If extension was sufficient then lithospheric thinning may have resulted in further mantle upwelling, enhancing the degree of melting and the volume of melt produced at Mt Kinabalu. The Linhaisai minette was emplaced as a series of dykes with a broad northerly trend (Bergman *et al.*, 1988), suggesting there was also extension in central Borneo at this time. The Linhaisai minette dykes represent a more restricted event with a lower degree of partial melting, which is suggested not only by its restricted, preserved volume but also by its silica-undersaturated composition. Such magmatism would transport

limited heat into the crust, which is consistent with the lack of evidence for crustal contamination here (Bergman *et al.,* 1988). Taken together, the two localities are consistent with an origin as intraplate, mafic magmatism. The major distinction is that at Mt Kinabalu there was a sufficient flux of magma, and heat, to promote melting of, and contamination by, the local upper crust.

Distribution of the EME-AFC Model

For application to other studies, a user-friendly spreadsheet of the EME-AFC model used in this study is available with instructions for download and utilisation in Supplementary Data 5 (both a blank template spreadsheet, 5a, and an example spreadsheet completed for Mt Kinabalu, 5b). Alternatively, access the spreadsheet at https://github.com/Alex-Burton-Johnson/EME-AFC-Modelling, or contact the lead author for the latest version.

CONCLUSIONS

- The primary magma of Mt Kinabalu was a partial melt of fertile, metasomatised, high-K, low-Na mantle. This may have been similar to the source for the contemporaneous Linhaisai minette magmatism in central Borneo, which would have resulted from lower degrees of melting. Magmatism was contemporaneous with and driven by regional crustal extension, possibly linked to slab roll-back during subduction of the Celebes Sea to the SE.

- Compiled experimental data shows that metaluminous melts with both Ca/Na > 1.5 and K/Na > 0.5 (Fig. 7), including Mt Kinabalu, cannot be generated through crustal anatexis.
- Fractional crystallisation of plagioclase, pyroxene, and amphibole rich cumulates from initial Mt Kinabalu magmas was accompanied by assimilation of partial melts of siliclastic sediments; most probably the basal units of the Crocker Formation. Combined with metasomatism of the mantle source, this imparted a high-K to shoshonitic chemistry to the granitoids. The fertility of the contaminating crust reduced after emplacement of the initial two granitic units, reducing the assimilation rate in subsequent magmatism. This variation in assimilation rate produced the geochemical heterogeneity of Mt Kinabalu.
- Evidence for the derivation of Mt Kinabalu granitic magmatism from assimilation and fractional crystallisation was determined through a new approach to AFC modelling of major and trace elements, and radiogenic and stable isotope ratios. The major and minor element chemistry of each fractionating phase is calculated to be in magmatic equilibrium using experimentally derived two-component partition coefficients at each stage of this incremental model (Equilibrated Major Element Assimilation and Fractional Crystallisation modelling, EME-AFC).

ACKNOWLEDGEMENTS

We thank Wendy Bohrson, Frank Spera, Hervé Rezeau, and an anonymous reviewer for their thorough reviews of this paper, and Wendy Bohrson and Marjorie Wilson for their work as editors. We are additionally indebted to Wendy Bohrson for her discussions during revision of the manuscript. We wish to thank Alim Biun, Felix

Tongkul and Maklarin Lakim for their assistance in facilitating the field season; Jamili Nais of Sabah Parks who allowed us to work in the National Park; the mountain guides and researchers of Mt Kinabalu National Park, especially Alijen "Jen", Halli, Jasirin, Sokaibin, Maklarin Lakim, Sapinus, Samuel and Nicholas; and we thank Robert Hall, Mike Cottam and the SE Asia Research Group at Royal Holloway for their support throughout this project.

FUNDING

NERC supported this study through a PhD studentship to AB-J and access to the Isotope Community Support Facility at SUERC.

REFERENCES

Alonso-Perez, R., Müntener, O. & Ulmer, P. (2008). Igneous garnet and amphibole fractionation in the roots of island arcs: experimental constraints on andesitic liquids. *Contributions to Mineralogy and Petrology* **157**, 541–558.

Beard, J. S. & Lofgren, G. E. (1991). Dehydration Melting and Water-Saturated Melting of Basaltic and Andesitic Greenstones and Amphibolites at 1, 3, and 6. 9 kb. *Journal of Petrology* **32**, 365–401.

Bergman, S. C., Dunni, D. P., Krol, L. G. & Colorado, U. S. A. (1988). Rock and mineral chemistry of the Linhaisai minette and the origin of Borneo diamonds, Central Kalimantan, Indonesia. *Canadian Minoalogist* **26**, 23–43.

Bogaerts, M., Scaillet, B. & Auwera, J. V. (2006). Phase Equilibria of the Lyngdal Granodiorite (Norway): Implications for the Origin of Metaluminous Ferroan Granitoids. *Journal of Petrology* **47**, 2405–2431.

Burton-Johnson, A. (2013). Origin, Emplacement and Tectonic Relevance of the Mt. Kinabalu Granitic Pluton of Sabah, Borneo. PhD Thesis, Durham University. http://etheses.dur.ac.uk/9450/.

Burton-Johnson, A., Macpherson, C. G. & Hall, R. (2017). Internal structure and emplacement mechanism of composite plutons: evidence from Mt Kinabalu, Borneo. *Journal of the Geological Society* **174**, 180–191.

Burton-Johnson, A., Stevenson, C. T. E., Macpherson, C. G., Harrison, R. J. & Muraszko, J. R. (In Prep.). Tectonic strain recorded by magnetic fabrics (AMS) in plutons: A tool to explore past tectonic regimes and syn-magmatic deformation. *Geological Society of America Bulletin*.

Castillo, P. R., Rigby, S. J. & Solidum, R. U. (2007). Origin of high field strength element enrichment in volcanic arcs: Geochemical evidence from the Sulu Arc, southern Philippines. *Lithos* **97**, 271–288.

Chappell, B. W. & White, a. J. R. (2011). I- and S-type granites in the Lachlan Fold Belt. *Transactions of the Royal Society of Edinburgh: Earth Sciences* **83**, 1–26.

Charlier, B. L. a., Ginibre, C., Morgan, D., Nowell, G. M., Pearson, D. G., Davidson, J. P. & Ottley, C. J. (2006). Methods for the microsampling and high-precision analysis of strontium and rubidium isotopes at single crystal scale for petrological and geochronological applications. *Chemical Geology* **232**, 114–133.

Chen, C.-H., Lee, C.-Y. & Shinjo, R. (2008). Was there Jurassic paleo-Pacific subduction in South China?: Constraints from 40Ar/39Ar dating, elemental and Sr–Nd–Pb isotopic geochemistry of the Mesozoic basalts. *Lithos* **106**, 83–92.

Chung, S.-L., Cheng, H., Jahn, B., O'Reilly, S. Y. & Zhu, B. (1997). Major and trace element, and Sr-Nd isotope constraints on the origin of Paleogene volcanism in South China prior to the South China Sea opening. *Lithos* **40**, 203–220.

Clemens, J. D. & Benn, K. (2010). Anatomy, emplacement and evolution of a shallow-level, post-tectonic laccolith: the Mt Disappointment pluton, SE Australia. *Journal of the Geological Society* **167**, 915–941.

Clemens, J. D. & Mawer, C. K. (1992). Granitic magma transport by fracture propagation. *Tectonophysics* **204**, 339–360.

Collenette, P. (1965). The geology and mineral resources of the Pensiangan and Upper Kinabatangan area, Sabah. *Malaysia Geological Survey Borneo Region, Memoir 12* 150.

Cottam, M. A., Hall, R., Sperber, C. & Armstrong, R. (2010). Pulsed emplacement of the Mount Kinabalu granite, northern Borneo. *Journal of the Geological Society* **167**, 49–60.

Cottam, M. A., Hall, R., Sperber, C., Kohn, B. P., Forster, M. A. & Batt, G. E. (2013). Neogene rock uplift and erosion in northern Borneo: evidence from the Kinabalu granite, Mount Kinabalu. *Journal of the Geological Society* **170**, 805–816.

Cox, K. G., Bell, J. D. & Pankhurst, R. J. (1979). *The interpretation of igneous rocks*. London, UK: George, Allen and Unwin.

Cullen, A., Macpherson, C., Taib, N. I., Burton-Johnson, A., Geist, D., Spell, T. & Banda, R. M. (2013). Age and petrology of the Usun Apau and Linau Balui volcanics: Windows to central Borneo's interior. *Journal of Asian Earth Sciences* **76**, 372–388.

Darbyshire, D. P. F. & Sewell, R. J. (1997). Nd and Sr isotope geochemistry of plutonic rocks from Hong Kong: implications for granite petrogenesis, regional structure and crustal evolution. *Chemical Geology* **143**, 81–93.

Deer, W. A., Howie, R. A., Zussman, J. & others (1992). *An introduction to the rock-forming minerals*. Longman Scientific & Technical Hong Kong.

DePaolo, D. J. (1981). Trace element and isotopic effects of combined wallrock assimilation and fractional crystallization. *Earth and planetary science letters* **53**, 189–202.

Dhonau, T. J. & Hutchison, C. S. (1965). The Darvel Bay area, East Sabah, Malaysia. *Malaysia Geological Survey Borneo Region, Annual Report for 1965* 141–160.

Douce, A. & Beard, J. S. (1995). Dehydration-melting of Biotite Gneiss and Quartz Amphibolite from 3 to 15 kbar. *Journal of Petrology* **36**, 707–738.

Douce, A. E. P. & Johnston, A. D. (1991). Phase equilibria and melt productivity in the pelitic system: implications for the origin of peraluminous granitoids and aluminous granulites. *Contributions to Mineralogy and Petrology* **107**, 202–218.

Galer, S. J. G. (1997). Optimal triple spiking for high precision lead isotope ratio determination. *Terra Nova* **9**, 441.

Gardien, V., Thompson, A. B., Grujic, D. & Ulmer, P. (1995). Experimental melting of biotite + plagioclase + quartz ± muscovite assemblages and implications for crustal melting. *Journal of Geophysical Research* **100**, 15581–15581.

Gardien, V., Thompson, A. & Ulmer, P. (2000). Melting of biotite+ plagioclase+ quartz gneisses: the role of H2O in the stability of amphibole. *Journal of Petrology* **41**, 651–666.

Ghiorso, M. S. & Sack, R. O. (1995). Chemical mass transfer in magmatic processes IV. A revised and internally consistent thermodynamic model for the interpolation and extrapolation of liquid-solid equilibria in magmatic systems at elevated temperatures and pressures. *Contributions to Mineralogy and Petrology* **119**, 197–212.

Gill, R. (1997). Modern Analytical Geochemistry: an introduction to quantitative chemical analysis techniques for Earth, environmental and materials scientists. Addison Wesley Longman.

Grove, T. L. & Donnelly-Nolan, J. M. (1986). The evolution of young silicic lavas at Medicine Lake Volcano, California: Implications for the origin of

compositional gaps in calc-alkaline series lavas. *Contributions to Mineralogy and Petrology* **92**, 281–302.

Grove, T. L., Elkins-Tanton, L. T., Parman, S. W., Chatterjee, N., Müntener, O. & Gaetani, G. a. (2003). Fractional crystallization and mantle-melting controls on calc-alkaline differentiation trends. *Contributions to Mineralogy and Petrology* **145**, 515–533.

Hall, R. (1996). Reconstructing Cenozoic SE Asia. In: Hall, R. & Blundell, D. J. (eds) *Tectonic Evolution of SE Asia*, 153–184.

Hall, R. (2013). Contraction and extension in northern Borneo driven by subduction rollback. *Journal of Asian Earth Sciences* **76**, 399–411.

Hall, R. & Wilson, M. E. J. (2000). Neogene sutures in eastern Indonesia. *Journal of Asian Earth Sciences* **18**, 781–808.

Hart, S. (1984). A large-scale isotope anomaly in the Southern Hemisphere mantle. *Nature*.

Hirata, T. (1996). Lead Isotopic Analyses of NIST Standard Reference Materials Using Multiple Collector Inductively Coupled Plasma Mass Spectrometry Coupled With a Modified External Correction Method for Mass Discrimination Effect. *Analyst* **121**, 1407–1411.

Hoang, N., Flower, M. & Carlson, R. (1996). Major, trace element, and isotopic compositions of Vietnamese basalts: Interaction of hydrous EM1-rich asthenosphere with thinned Eurasian lithosphere. *Geochimica et Cosmochimica Acta* **60**, 4329–4351.

Hutchison, C. (2000). A Miocene collisional belt in north Borneo: uplift mechanism and isostatic adjustment quantified by thermochronology. *Journal of the Geological Society* **157**, 783–793.

Hutchison, C. S. (1996). The "Rajang accretionary prism" and "Lupar Line" problem of Borneo. *Geological Society, London, Special Publications* **106**, 247–261.

Jagoutz, O. E., Burg, J.-P., Hussain, S., Dawood, H., Pettke, T., Iizuka, T. & Maruyama, S. (2009). Construction of the granitoid crust of an island arc part I: geochronological and geochemical constraints from the plutonic Kohistan (NW Pakistan). *Contributions to Mineralogy and Petrology* **158**, 739.

Kirk, H. J. C. (1968). *The igneous rocks of Sarawak and Sabah*. US Government Printing Office.

Koopmans, B. N. (1967). Deformation of the metamorphic rocks and the Chert–Spilite Formation in the southern part of the Darvel Bay area, Sabah. *Geological Survey of Malaysia, Borneo Region, Bulletin* **8**, 14–24.

Kudrass, H. R., Muller, P., Kreuzer, H. & Weiss, W. (1990). Volcanic rocks and tertiary carbonates dredged from the Cagayan Ridge and the Southwest Sulu

Sea, Philippines. *Rangin, C, Silver, EA, von Breymann, MT, et al., Proc. ODP, Init. Repts*, 93–100.

Lackey, J. S., Valley, J. W., Chen, J. H. & Stockli, D. F. (2008). Dynamic Magma Systems, Crustal Recycling, and Alteration in the Central Sierra Nevada Batholith: the Oxygen Isotope Record. *Journal of Petrology* **49**, 1397–1426.

Le Maitre, R. W. et al. (1989). A classification of igneous rocks and glossary of terms. Oxford: Blackwell Publishing.

Leong, K. M. (1974). The geology and mineral resources of the Upper Segama Valley and Darvel Bay area, Sabah, Malaysia. US Government Printing Office.

Leuthold, J., Muntener, O., Baumgartner, L. P., Putlitz, B. & Chiaradia, M. (2012). A Detailed Geochemical Study of a Shallow Arc-related Laccolith; the Torres del Paine Mafic Complex (Patagonia). *Journal of Petrology* **54**, 273–303.

Liew, T. & McCulloch, M. (1985). Genesis of granitoid batholiths of Peninsular Malaysia and implications for models of crustal evolution: Evidence from a Nd-Sr isotopic and U-Pb zircon study. *Geochimica et Cosmochimica Acta*.

Macpherson, C. G., Chiang, K. K., Hall, R., Nowell, G. M., Castillo, P. R. & Thirlwall, M. F. (2010). Plio-Pleistocene intra-plate magmatism from the southern Sulu Arc, Semporna peninsula, Sabah, Borneo: Implications for high-Nb basalt in subduction zones. *Journal of Volcanology and Geothermal Research* **190**, 25–38.

Macpherson, C. G. & Mattey, D. P. (1998). Oxygen isotope variations in Lau Basin lavas. *Chemical Geology* **144**, 177–194.

Mattey, D., Lowry, D. & Macpherson, C. (1994). Oxygen isotope composition of mantle peridotite. *Earth and Planetary Science Letters* **128**, 231–241.

Mattey, D. & Macpherson, C. (1993). High-precision oxygen isotope microanalysis of ferromagnesian minerals by laser-fluorination. *Chemical Geology* **105**, 305–318.

McCaffrey, K. J. W. & Petford, N. (1997). Are granitic intrusions scale invariant? *Journal of the Geological Society* **154**, 1–4.

Montel, J.-M. & Vielzeuf, D. (1997). Partial melting of metagreywackes, Part II. Compositions of minerals and melts. *Contributions to Mineralogy and Petrology* **128**, 176–196.

Nandedkar, R. H., Ulmer, P. & Müntener, O. (2014). Fractional crystallization of primitive, hydrous arc magmas: an experimental study at 0.7 GPa. *Contributions to Mineralogy and Petrology* **167**, 1015.

Naney, M. (1983). Phase equilibria of rock-forming ferromagnesian silicates in granitic systems. *American Journal of Science* **283**, 993–1033.

Nowell, G. M., Pearson, D. G., Ottley, C. J., Schweiters, J. & Dowall, D. (2003). Long-term performance characteristics of a plasma ionisation multi-collector mass spectrometer (PIMMS): the ThermoFinnigan Neptune. *Plasma Source Mass Spectrometry: Applications and Emerging Technologies. Cambridge: Royal Society of Chemistry* 307–320.

Ottley, C., Pearson, D. & Irvine, G. (2003). A routine method for the dissolution of geological samples for the analysis of REE and trace elements via ICP-MS. *Plasma source mass …*.

Patino Douce, a. E. (2004). Vapor-Absent Melting of Tonalite at 15-32 kbar. *Journal of Petrology* **46**, 275–290.

Petford, N. & Clemens, J. (2000). Granites are not diapiric! *Geology Today* **16**, 180–184.

Petford, N., Cruden, A. R., McCaffrey, K. J. & Vigneresse, J. L. (2000). Granite magma formation, transport and emplacement in the Earth's crust. *Nature* **408**, 669–73.

Rangin, C. & Silver, E. A. (1990). Geological setting of the Celebes and Sulu Seas. In: Silver, E. A., Rangin, C. & von Breymann, M. T. (eds) *Proceedings of the Ocean Drilling Program, Initial Reports 124*, 35–42.

Rapp, R. P. & Watson, E. B. (1995). Dehydration Melting of Metabasalt at 8-32 kbar: Implications for Continental Growth and Crust-Mantle Recycling. *Journal of Petrology* **36**, 891–931.

Rapp, R. P., Watson, E. B. & Miller, C. F. (1991). Partial melting of amphibolite/eclogite and the origin of Archean trondhjemites and tonalites. *Precambrian Research* **51**, 1–25.

Reinhard, M. & Wenk, E. (1951). Geology of the Colony of North Borneo. *British Borneo Geological Survey Bulletin* **1**.

Royse, K. R., Kempton, P. D. & Darbyshire, D. P. F. (1998). Procedure for the analysis of rubidium–strontium and samarium–neodymium isotopes at the NERC Isotope Geosciences Laboratory. *NIGL Report Series* **121**, 28.

Rudnick, R. & Gao, S. (2003). Composition of the continental crust. *Treatise on geochemistry* **3**, 1–64.

Rushmer, T. (1991). Partial melting of two amphibolites: contrasting experimental results under fluid-absent conditions. *Contributions to Mineralogy and Petrology* **107**, 41–59.

Rushmer, T. (1993). Experimental high-pressure granulites: some applications to natural mafic xenolith suites and Archean granulite terranes. *Geology* **21**, 411–414.

Sen, C. & Dunn, T. (1994). Dehydration melting of a basaltic composition amphibolite at 1.5 and 2.0 GPa: implications for the origin of adakites. *Contributions to Mineralogy and Petrology* **117**, 394–409.

Singh, J. & Johannes, W. (1996A). Dehydration melting of tonalites. Part I. Beginning of melting. *Contributions to Mineralogy and Petrology* **125**, 16–25.

Singh, J. & Johannes, W. (1996B). Dehydration melting of tonalites. Part II. Composition of melts and solids. *Contributions to Mineralogy and Petrology* **125**, 26–44.

Sisson, T. W., Ratajeski, K., Hankins, W. B. & Glazner, A. F. (2005). Voluminous granitic magmas from common basaltic sources. *Contributions to Mineralogy and Petrology* **148**, 635–661.

Skjerlie, K. P. & Johnston, A. D. (1992). Vapor-absent melting at 10 kbar of a biotite- and amphibole-bearing tonalitic gneiss : Implications for the generation of A-type granites. *Geology* **20**, 263–266.

Smith, T. E., Huang, C. H. & Sajona, F. G. (1988). Geochemistry and petrogenesis of the volcanic rocks from holes 768 and 769, Sulu Sea. *Proceedings of the Ocean Drilling Program: Scientific results*. The Program, 297.

Spadea, P., D'Antonio, M. & Thirlwall, M. F. (1996). Source characteristics of the basement rocks from the Sulu and Celebes Basins (Western Pacific): chemical and isotopic evidence. *Contributions to Mineralogy and Petrology* **123**, 159–176.

Spera, F. J. & Bohrson, W. A. (2001). Energy-constrained open-system magmatic processes I: general model and energy-constrained assimilation and fractional crystallization (EC-AFC) formulation. *Journal of Petrology* **42**, 999–1018.

Suggate, S. M., Cottam, M. A., Hall, R., Sevastjanova, I., Forster, M. A., White, L. T., Armstrong, R. a., Carter, A. & Mojares, E. (2013). South China continental margin signature for sandstones and granites from Palawan, Philippines. *Gondwana Research*.

Sun, S. -s. & McDonough, W. F. (1989). Chemical and isotopic systematics of oceanic basalts: implications for mantle composition and processes. *Geological Society, London, Special Publications* **42**, 313–345.

Taylor, B. & Hayes, D. E. (1983). Origin and history of the South China Sea basin. In: Hayes, D. E. (ed.) *The Tectonic and Geologic Evolution of Southeast Asian Seas and Islands: Part 2*, 23–56.

Thirlwall, M. (1991). Long-term reproducibility of multicollector Sr and Nd isotope ratio analysis. *Chemical Geology: Isotope Geoscience section* **94**, 85–104.

Thuy, N. T. B., Satir, M., Siebel, W., Vennemann, T. & Long, T. V. (2004). Geochemical and isotopic constraints on the petrogenesis of granitoids from the Dalat zone, southern Vietnam. *Journal of Asian Earth Sciences* **23**, 467–482.

Tongkul, F. (1991). Tectonic evolution of Sabah, Malaysia. *Journal of Southeast Asian Earth Sciences* **6**, 395–405.

Tongkul, F. (1994). The geology of Northern Sabah, Malaysia: its relationship to the opening of the South China Sea Basin. *Tectonophysics* **235**, 131–147.

Tu, K., Flower, M., Carlson, R. & Xie, G. (1992). Magmatism in the South China Basin: 1. Isotopic and trace-element evidence for an endogenous Dupal mantle component. *Chemical ...* **97**, 47–63.

van Hattum, M. W., Hall, R., Pickard, A. L. & Nichols, G. J. (2006). Southeast Asian sediments not from Asia: Provenance and geochronology of north Borneo sandstones. *Geology* **34**, 589–592.

Vielzeuf, D. & Holloway, J. (1988). Experimental determination of the fluid-absent melting relations in the pelitic system. *Contributions to Mineralogy and Petrology* 257–276.

Wang, Y., Fan, W., Cawood, P. a. & Li, S. (2008). Sr–Nd–Pb isotopic constraints on multiple mantle domains for Mesozoic mafic rocks beneath the South China Block hinterland. *Lithos* **106**, 297–308.

Winther, K. T. (1996). An experimentally based model for the origin of tonalitic and trondhjemitic melts. *Chemical Geology* **127**, 43–59.

Wolf, M. B. & Wyllie, P. J. (1994). Dehydration-melting of amphibolite at 10 kbar: the effects of temperature and time. *Contributions to Mineralogy and Petrology* **115**, 369–383.

Xiao, L. & Clemens, J. D. (2007). Origin of potassic (C-type) adakite magmas: Experimental and field constraints. *Lithos* **95**, 399–414.

Xiong, X. L., Adam, J. & Green, T. H. (2005). Rutile stability and rutile/melt HFSE partitioning during partial melting of hydrous basalt: Implications for TTG genesis. *Chemical Geology* **218**, 339–359.

Yan, Q. & Shi, X. (2009). Mineralogy, Pb and O isotopic characteristics of granitic rocks from the Nansha block (South China Sea): magmatic process and tectonic affiliation. *AGU Fall Meeting Abstracts*, 2133.

Yan, Q., Shi, X. & Li, N. (2011). Oxygen and lead isotope characteristics of granitic rocks from the Nansha block (South China Sea): Implications for their petrogenesis and tectonic affinity. *Island arc* **20**, 150–159.

Yan, Q., Shi, X., Liu, J., Wang, K. & Bu, W. (2010). Petrology and geochemistry of Mesozoic granitic rocks from the Nansha micro-block, the South China Sea: Constraints on the basement nature. *Journal of Asian Earth Sciences* **37**, 130–139.

Yan, Q., Shi, X., Wang, K., Bu, W. & Xiao, L. (2008). Major element, trace element, and Sr, Nd and Pb isotope studies of Cenozoic basalts from the South China Sea. *Science in China Series D: Earth Sciences* **51**, 550–566.

Yanbo, C. & Jingwen, M. (2010). Age and geochemistry of granites in Gejiu area, Yunnan province, SW China: Constraints on their petrogenesis and tectonic setting. *Lithos* **120**, 258–276.

Zhou, X., Sun, T., Shen, W., Shu, L. & Niu, Y. (2006). Petrogenesis of Mesozoic granitoids and volcanic rocks in South China: a response to tectonic evolution. *Episodes* 26–33.

Zhu, B. (1995). The mapping of geochemical provinces in China based on Pb isotopes. *Journal of Geochemical Exploration* **55**, 171–181.

Zindler, a & Hart, S. (1986). Chemical Geodynamics. *Annual Review of Earth and Planetary Sciences* **14**, 493–571.

Zou, H. & Fan, Q. (2010). U–Th isotopes in Hainan basalts: Implications for sub-asthenospheric origin of EM2 mantle endmember and the dynamics of melting beneath Hainan Island. *Lithos* **116**, 145–152.

Zou, H., Zindler, A., Xu, X. & Qi, Q. (2000). Major, trace element, and Nd, Sr and Pb isotope studies of Cenozoic basalts in SE China: mantle sources, regional variations, and tectonic significance. *Chemical Geology* **171**, 33–47.

FIGURE CAPTIONS

Fig. 1. (a) Regional geography of Mt Kinabalu and the locations referred to in the text within SE Asia. (b) Aerial photograph of Mt Kinabalu from the south highlighting its extreme vertical relief; courtesy of Tony Barber. (c) Internal structure and U-Pb zircon emplacement ages of the Mt Kinabalu intrusion (Cottam *et al.*, 2010; Burton-Johnson *et al.*, 2017). Volumes were determined using field relations and contact orientations, as discussed in Burton-Johnson *et al.* (2017). Abbreviations: Tn – Tonalite, Gd – Granodiorite, Gt – Granite, Pph – Porphyritic Granite.

Fig. 2. Geochemical classification diagrams of the Mt Kinabalu granitoids. (a) TAS diagram of Cox *et al.* (1979). (b) K_2O *vs* silica diagram of Le Maitre *et al.* (1989). Abbreviations as in Fig. 1. Existing data shown for comparison (Vogt & Flower, 1989).

Fig. 3. Amphibole compositions, following the Leake *et al.* (1997) classification for calcic amphiboles.

Fig. 4. Multi-element, primitive mantle-normalised trace element patterns and chondrite normalised REE patterns for the Mt Kinabalu granitic units. The upper and lower 95% confidence limits for each unit are indicated. Normalising values from Sun & McDonough (1989). Abbreviations as in Fig. 1.

Fig. 5. Sr, Nd and Pb isotope ratios of Mt Kinabalu granitic rocks at 7.5Ma. Data for comparison: South China Sea basalts (Tu *et al.*, 1992; Yan *et al.*, 2008); Mesozoic granites of the South China Block and Yangtze Block (Zhu, 1995); Mesozoic granitoids of Vietnam (Thuy *et al.*, 2004), Hong Kong (Darbyshire & Sewell, 1997) and Yunnan Province (Yanbo & Jingwen, 2010); Neogene basalts from Borneo (Macpherson *et al.*, 2010; Cullen *et al.*, 2013); Mesozoic granites from the South China Sea (Yan *et al.*, 2010, 2011); Spreading centre basalts of the Indian Ocean from the PetDB database (http://www.earthchem.org/petdb); Northern Hemisphere Reference line (NHRL) back-calculated to 7.5Ma using the mean U and Pb concentrations of the I-MORB data (Hart, 1984). EM2 fields from Zindler & Hart (1986). Bulk Silicate Earth (BSE) from Faure (1986). Abbreviations as in Fig. 1.

Fig. 6. $\delta^{18}O$ values of quartz and hornblende in Mt Kinabalu rocks. 2SD error bars based on replicate analyses of each mineral from the same sample. Calculated isotherms and associated errors (grey shaded regions) shown for the whole-rock

solidus and hornblende crystallisation temperatures for the vapour saturated 200MPa experiments of Naney (1983) (calculated from Clayton *et al.*, 1989; Kohn & Valley, 1998; Chacko *et al.*, 2001; Valley, 2003; Lackey *et al.*, 2008). Abbreviations as in Fig. 1.

Fig. 7. Comparison of the Mt Kinabalu data with collated data for melting experiments on potential felsic sources (tonalites and felsic gneisses), mafic sources (basalts and basaltic amphibolites), and sedimentary sources (sediments and metasediments) (Vielzeuf & Holloway, 1988; Beard & Lofgren, 1991; Douce & Johnston, 1991; Rapp *et al.*, 1991; Rushmer, 1991, 1993; Winther & Newton, 1991; Skjerlie & Johnston, 1992; Sen & Dunn, 1994; Wolf & Wyllie, 1994; Douce & Beard, 1995; Gardien *et al.*, 1995, 2000; Rapp & Watson, 1995; Singh & Johannes, 1996a, 1996b; Winther, 1996; Montel & Vielzeuf, 1997; Patino Douce, 2004; Sisson *et al.*, 2005; Xiong *et al.*, 2005; Xiao & Clemens, 2007). Note that the samples from mafic sources showing Ca/Na values >3 (highlighted in circles) are peraluminous with high Al/(Na+K) values. Crustal values from Rudnick & Gao (2003). Abbreviations as in Fig. 1.

Fig. 8. Temperature *vs* SiO_2 for glasses from published crystallisation experiments and empirical relationship derived by linear regression (Villiger *et al.*, 2004; Villiger, 2005; Alonso-Perez *et al.*, 2009: 200; Krawczynski *et al.*, 2012; Nandedkar *et al.*, 2014).

Fig. 9. Liquid lines of descent (LLD) of major elements (wt %) for basalt SBK13 from Semporna, northeast Borneo (Macpherson *et al.*, 2010), compared with fractionating assemblages from Rhyolite-MELTS and EME-AFC models. Whole-rock (WR) compositions of the basaltic suite are shown for comparison (Macpherson *et al.*, 2010). Note that these are fractional crystallisation only models, and the discrepancy between the models and sample data in the Na_2O and K_2O plots highlights the effect of crustal assimilation on the differentiation of the Bornean basaltic suite (Macpherson *et al.*, 2010).

Fig. 10. Molar mass % of the analysed mineral chemistries of Mt Kinabalu and EME-AFC modelled mineral chemistries of the King Granite.

Fig. 11. Alkali metal compositions of Mt Kinabalu granites and models to simulate assimilation with fractional crystallisation. (a) K_2O *versus* SiO_2, (b) Na_2O *versus* SiO_2, (c) K/Na *versus* Ca/Na. Model 1 (black): Linau Balui basalt (LB85; Cullen *et al*., 2013) contaminated by the bulk chemistry of a meta-conglomerate xenolith from the Donkey Granite. Model 2 (red): LB85 contaminated by partial melt of biotite, plagioclase and quartz-bearing starting material (BPQ) of Gardien *et al.* (1995): Model 3 (blue) Starting material with modified alkali contents as discussed in text contaminated by BPQ partial melt (as in Model 2). Experimental melt data in (c) as in Fig. 7. Neogene basalt data from Macpherson *et al.* (2010) and Cullen *et al.* (2013). Note that Model 1 is largely overlain by Model 2 in (c). Abbreviations as in Fig. 1.

Fig. 12. Compositional comparison (isotopes, trace elements and selected major elements) of the EME-AFC King Granite model end values, liquid line of descent (LLD), fractionating assemblage and bulk cumulate with the primary magma (2.1 wt % Na_2O and 2.5 wt % K_2O; Model 3 in Fig. 11), partially melted xenolith and partially melted BPQ assimilant (used respectively for trace and major elements) and King Granite target composition. Normalising values from Sun & McDonough (1989). Abbreviations as in Fig. 1.

Fig. 13. Probability density plots of $^{206}Pb/^{238}U$ inherited zircon ages from Mt Kinabalu (Cottam *et al.,* 2010) and $^{206}Pb/^{238}U$ detrital zircon ages from the principal sedimentary units of Sabah: the Eocene Sapulut and Trusmadi Formations and the Eocene-Oligocene units of the Crocker Formation (van Hattum *et al.,* 2013).

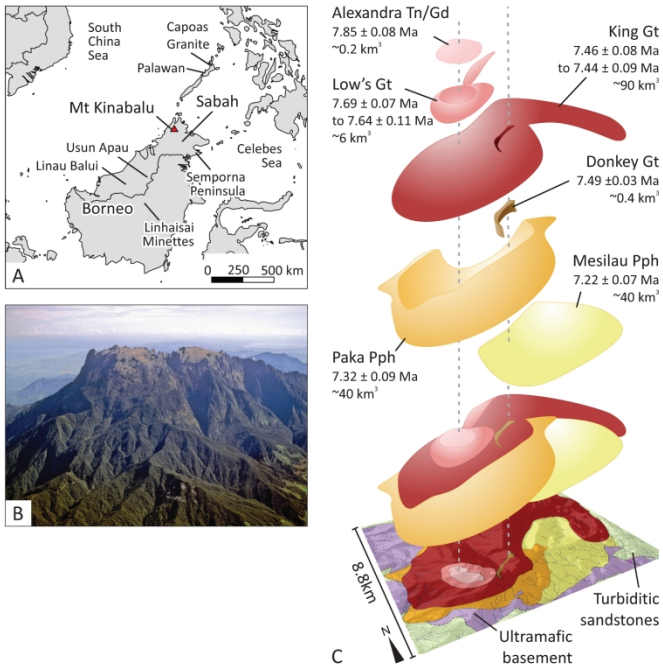

Fig. 1

296x209mm (300 x 300 DPI)

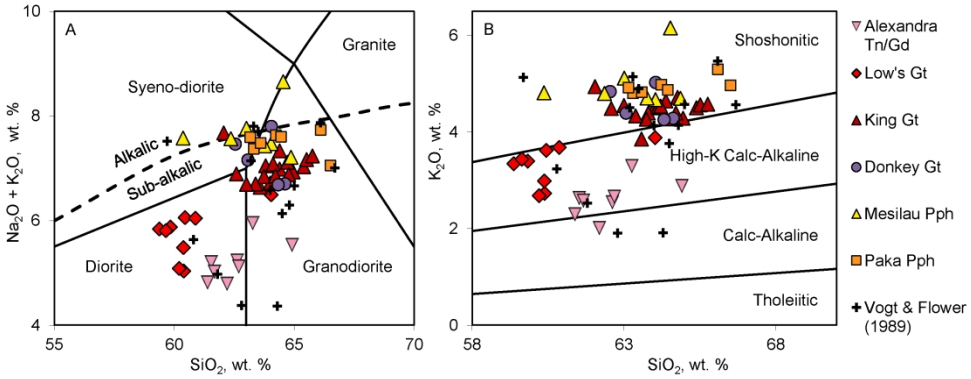

Fig. 2.

260x101mm (300 x 300 DPI)

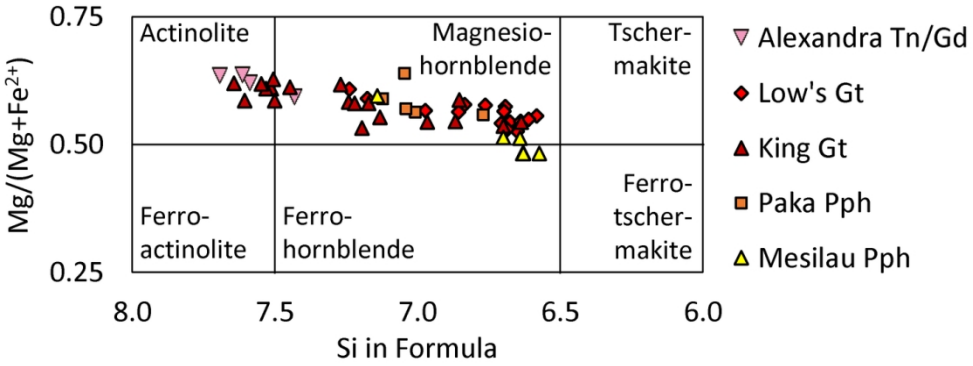

Fig. 3.

127x46mm (300 x 300 DPI)

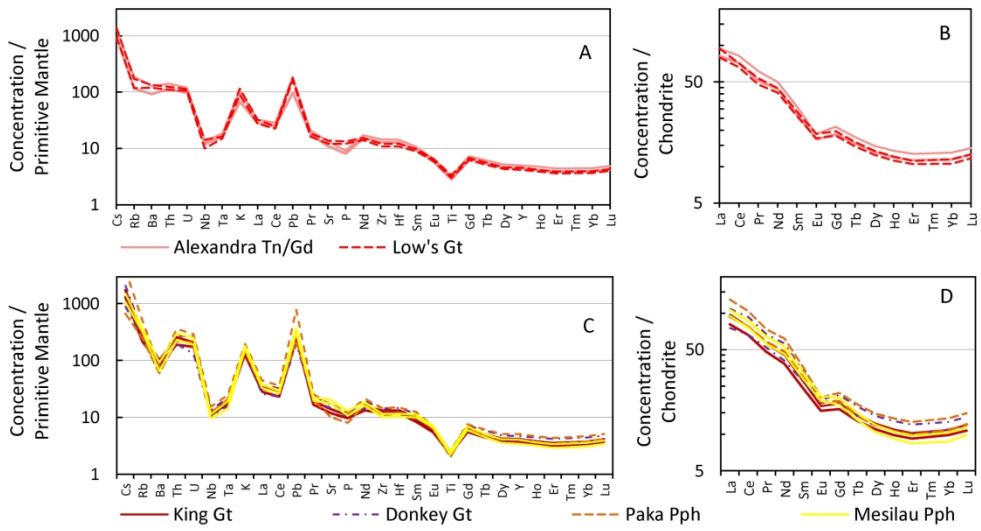

Fig. 4.

190x101mm (300 x 300 DPI)

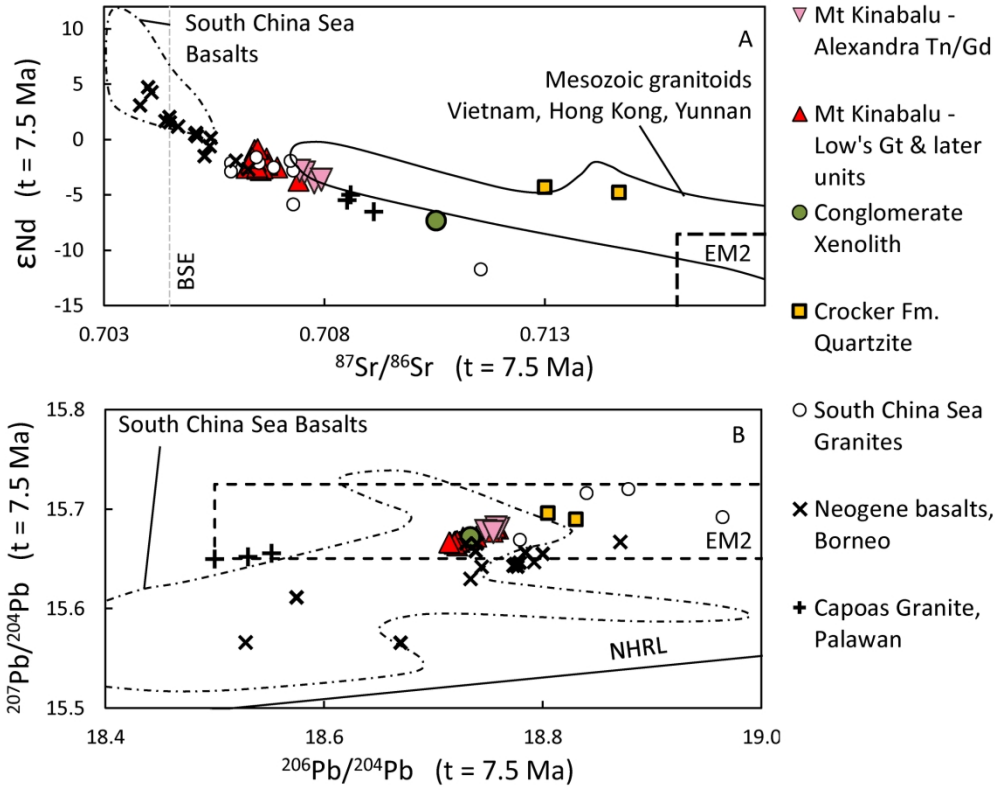

Fig. 5.

190x154mm (300 x 300 DPI)

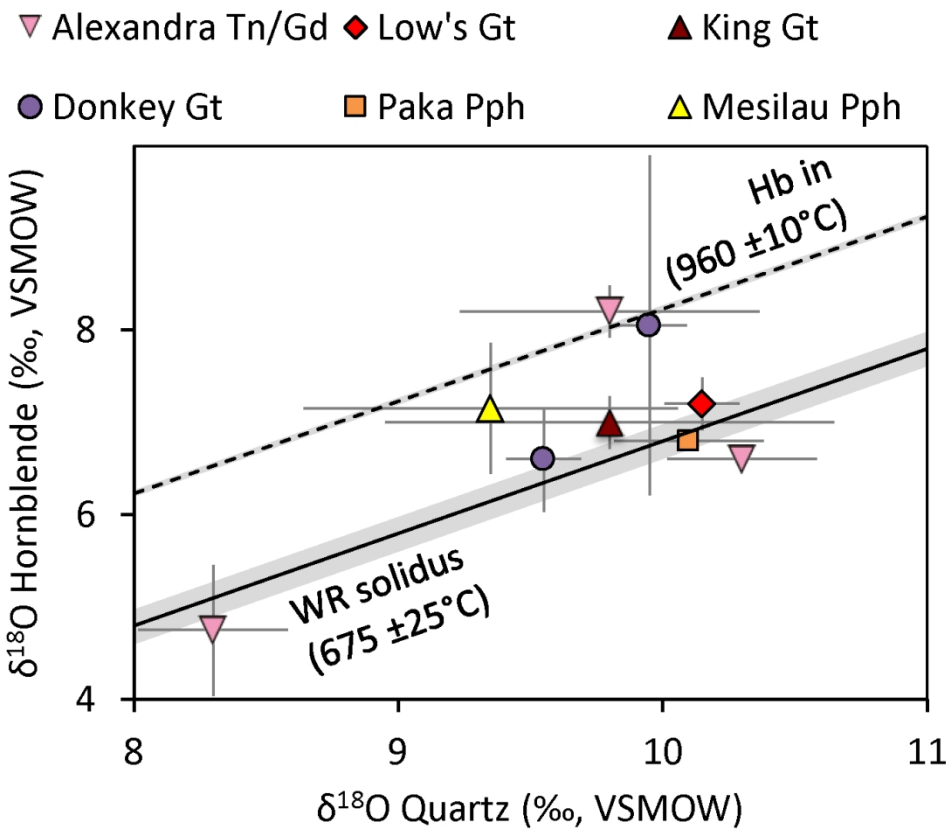

Fig. 6.

122x103mm (300 x 300 DPI)

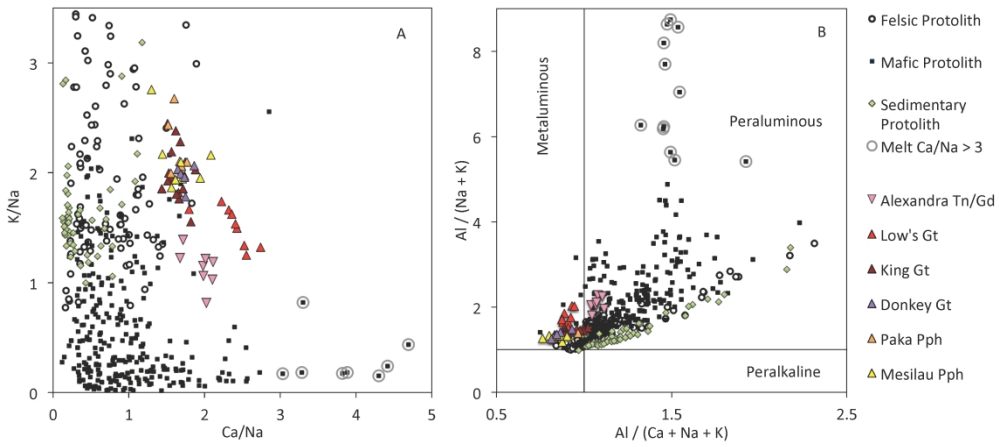

Fig. 7.

381x177mm (300 x 300 DPI)

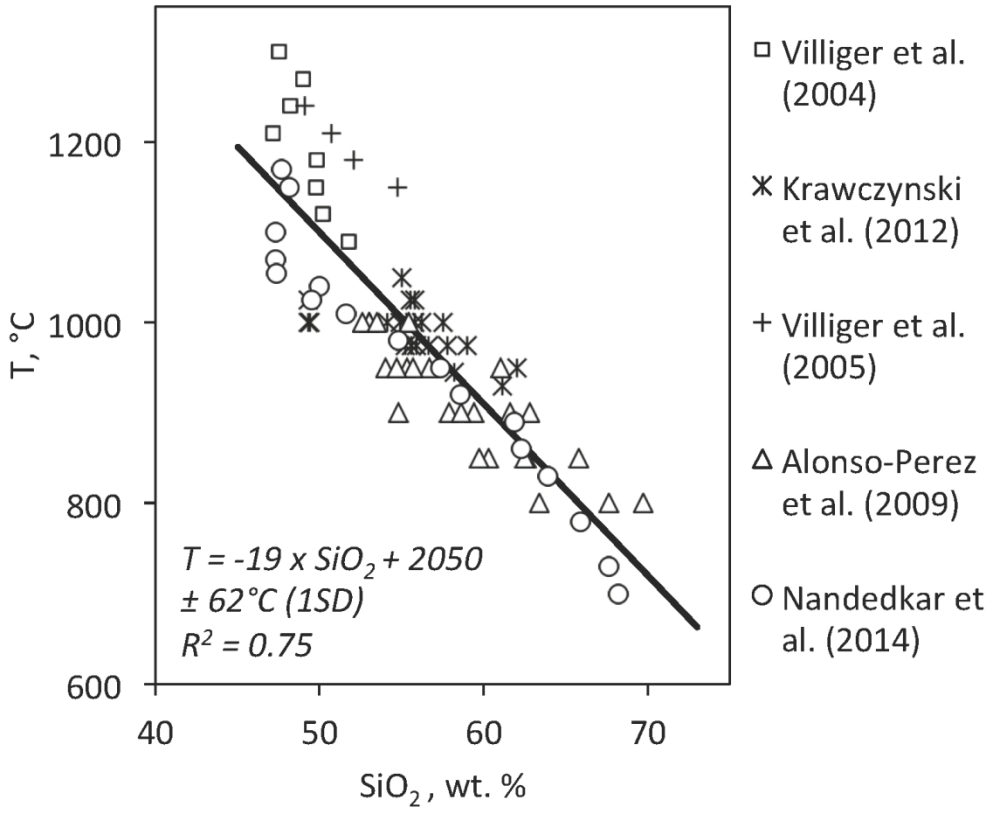

Fig. 8.

134x114mm (300 x 300 DPI)

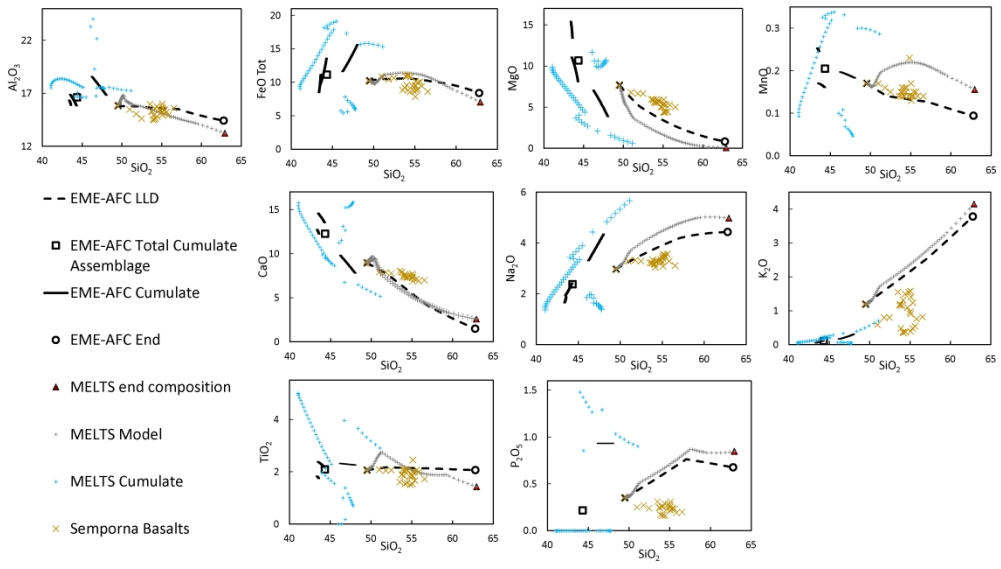

Fig. 9. Liquid lines of descent (LLD) of major elements (wt. %) for basalt SBK13 from Semporna, northeast Borneo (Macpherson et al., 2010), compared with fractionating assemblages from Rhyolite-MELTS and EME-AFC models. Whole rock (WR) compositions of the basaltic suite are shown for comparison (Macpherson et al., 2010). Note that these are fractional crystallisation only models, and the discrepancy between the models and sample data in the Na2O and K2O plots highlights the effect of crustal assimilation on the differentiation of the Bornean basaltic suite (Macpherson et al., 2010).

384x225mm (300 x 300 DPI)

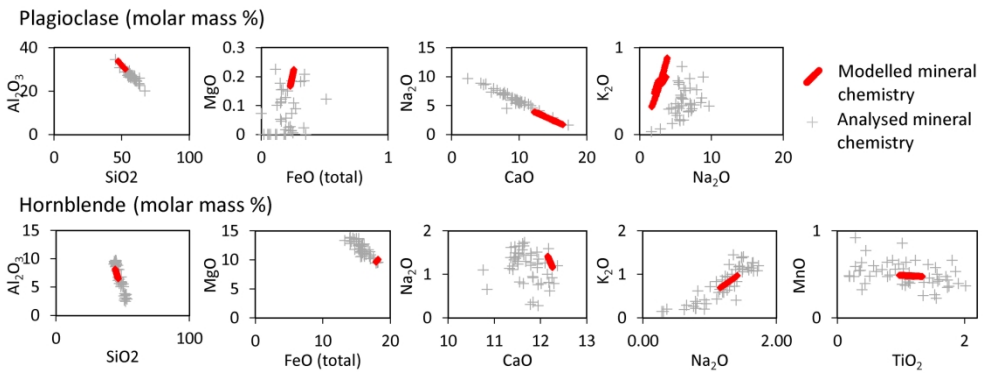

Fig. 10.

218x81mm (300 x 300 DPI)

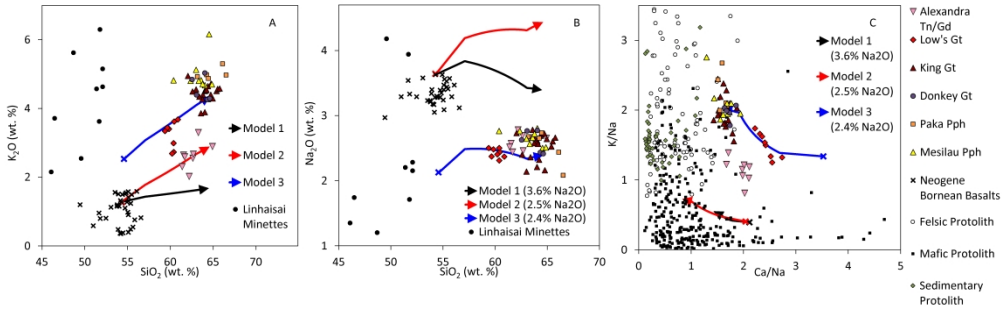

Fig. 11. Alkali metal chemistries of Mt Kinabalu granites and models to simulate assimilation with fractional crystallisation. (a) K2O versus SiO2, (b) Na2O versus SiO2, (c) K/Na versus Ca/Na. Model 1 (black): Linau Balui basalt (LB85; Cullen et al., 2013) contaminated by the bulk chemistry of meta-conglomerate xenolith from the Donkey Granite. Model 2 (red): LB85 contaminated by partial melt of biotite, plagioclase and quartz-bearing starting material (BPQ) of Gardien et al. (1995): Model 3 (blue) Starting material with modified alkali contents as discussed in text contaminated by BPQ partial melt (as in Model 2). Experimental melt data in (c) as in Fig. 7. Neogene basalt data from Macpherson et al. (2010) and Cullen et al. (2013). Note that Model 1 is larger overlain by Model 2 in (c). Abbreviations as in Fig. 1.

571x177mm (300 x 300 DPI)

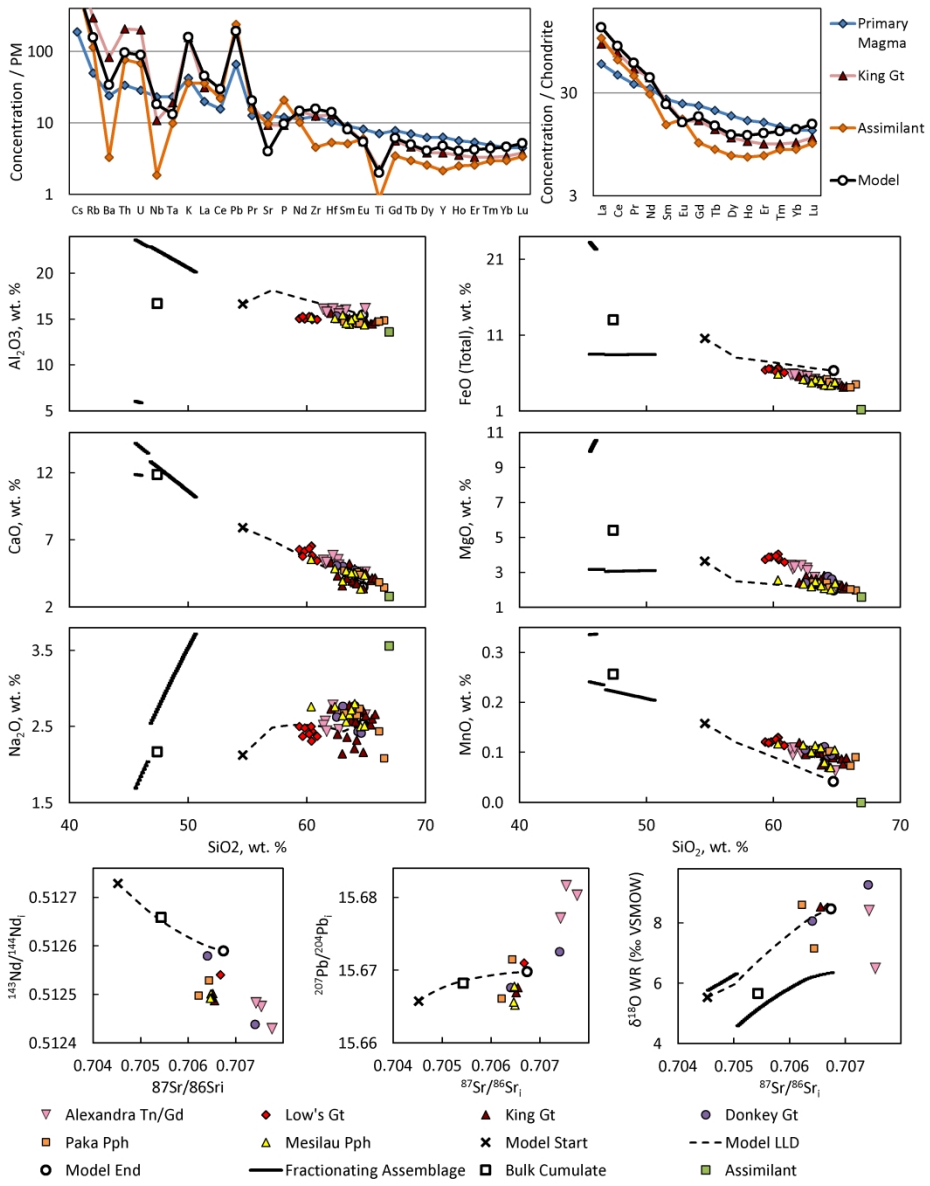

Fig. 12. Compositional comparison (isotopes, trace elements and selected major elements) of the EME-AFC King Granite model end values, liquid line of descent (LLD), fractionating assemblage and bulk cumulate with the primary magma (2.1% Na2O and 2.5% K2O; Model 3 in Fig. 11), partially melted xenolith and partially melted BPQ assimilant (used respectively for trace and major elements) and King Granite target composition. Normalising values from Sun and McDonough (1989). Abbreviations as in Fig. 1.

266x342mm (300 x 300 DPI)

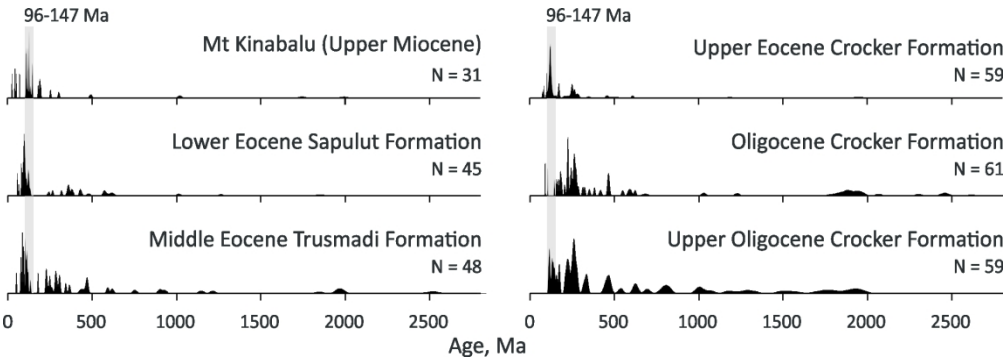
96-147 Ma
Mt Kinabalu (Upper Miocene)
N = 31
Lower Eocene Sapulut Formation
N = 45
Middle Eocene Trusmadi Formation
N = 48
96-147 Ma
Upper Eocene Crocker Formation
N = 59
Oligocene Crocker Formation
N = 61
Upper Oligocene Crocker Formation
N = 59
0
500
1000
1500
2000
2500
0
500
1000
1500
2000
2500
Age, Ma

Fig. 13.

Lat.	6.0728	6.0784	6.0763	6.0756	6.0790	6.0818	6.0767	6.0712	6.1235	6.0831	6.1224	6.0310	6.0750	6.0768	6.0788
Long.	116.5570	116.5513	116.5502	116.5537	116.5500	116.5492	116.5490	116.5533	116.5720	116.5538	116.5738	116.7251	116.5587	116.5571	116.5570
Height, m	4030	3827	3929	3959	3803	3684.11	3991.24	3891.51	2586	3945	0	0	4096	3947	3847
	Alex. Gd	Alex. Gd	Alex. Gd	Alex. Gd	Alex. Gd	Alex. Gd	Alex. Gd	Alex. Gd	Low's Gt	Low's Gt	Low's Gt	Low's Gt	Low's Gt	Low's Gt	Low's Gt
	CS016	CS021	CS022	CS023	CS036	A042	A047	A054	CS077	A046	A218	SBK121	CS018	CS019	CS020
(wt%)															
SiO_2	63.26	61.53	62.62	62.19	62.68	64.91	61.38	61.67	60.88	60.21	59.65	60.40	60.45	60.39	59.38
TiO_2	0.65	0.68	0.66	0.72	0.66	0.54	0.63	0.66	0.63	0.66	0.68	0.71	0.67	0.69	0.67
Al_2O_3	15.99	15.87	15.85	16.10	15.56	16.13	16.07	15.75	14.96	15.29	15.29	15.25	14.96	15.13	15.07
FeO_{TOT}	5.14	5.84	5.42	5.70	5.53	4.54	5.81	5.79	6.07	6.19	6.56	6.74	6.44	6.56	6.43
MnO	0.10	0.10	0.10	0.10	0.10	0.06	0.11	0.11	0.11	0.13	0.12	0.13	0.12	0.13	0.12
MgO	2.72	3.23	3.24	3.39	3.10	2.23	3.40	3.32	3.59	3.94	3.87	4.05	3.72	3.83	3.74
CaO	4.73	5.28	5.54	5.84	5.14	4.61	5.49	5.35	5.47	6.36	5.80	6.57	5.87	6.55	6.30
Na_2O	2.66	2.57	2.69	2.78	2.46	2.65	2.52	2.44	2.37	2.40	2.37	2.31	2.44	2.50	2.50
K_2O	3.30	2.64	2.55	2.02	2.67	2.89	2.31	2.59	3.68	2.69	3.44	2.73	3.62	2.99	3.34
P_2O_5	0.18	0.18	0.19	0.20	0.18	0.17	0.18	0.18	0.26	0.24	0.28	0.30	0.27	0.29	0.27
Total	99.30	99.44	99.46	99.67	99.53	99.90	107.60	99.42	99.75	99.84	100.02	99.94	99.28	99.79	99.12
LOI	0.73	0.87	0.57	1.00	0.84	0.66	1.06	0.92	1.05	1.05	1.23	1.24	0.50	0.93	0.58
ppm															
Ta	0.78	0.71	0.66	0.68	0.66	0.82	0.64	0.67	0.58	0.62	0.63	0.66	0.62	0.60	0.70
Sc	14.20	22.04	17.91	21.34	21.54	12.94	20.47	20.45	21.35	21.79	22.11	17.88	17.97	18.30	17.12
V	100.34	187.45	142.53	166.38	167.06	101.80	176.00	173.00	184.49	188.30	201.10	151.50	151.41	155.76	151.54
Cr	42.20	58.87	50.84	56.45	57.66	35.12	62.96	65.45	75.68	92.40	82.55	62.35	61.20	63.80	60.12
Ga	13.97	17.75	14.50	17.62	17.67	17.68	17.94	17.71	16.65	16.93	17.67	13.74	13.81	14.17	14.05
Co	10.89	15.47	13.14	15.11	15.29	10.71	16.32	16.01	20.25	20.39	20.47	16.33	16.95	17.04	16.47
Ni	24.91	16.65	18.99	15.39	14.60	11.44	17.18	16.82	18.23	22.27	20.15	13.11	14.60	13.89	13.14
Cu	3.73	35.34	12.23	5.12	23.57	7.39	22.66	17.64	43.11	28.37	52.02	1052.8	29.28	62.40	38.56
Zn	40.50	48.60	44.49	34.90	50.79	38.10	54.04	59.54	50.76	59.52	54.50	71.75	45.11	45.67	48.48
Cs	9.17	9.45	9.41	7.71	8.25	9.57	9.71	9.00	11.32	5.46	11.75	9.12	11.57	8.93	9.73
Rb	103.26	102.26	86.82	92.40	98.63	107.30	83.80	93.55	117.35	68.08	119.50	74.43	107.97	90.63	83.41
Ba	770.96	901.42	924.83	925.12	890.96	834.60	816.00	865.50	847.28	856.00	854.30	977.93	1010.8	867.50	863.25
Sr	193.66	239.28	214.07	249.52	248.24	255.50	247.10	257.90	273.97	310.30	300.70	243.30	238.73	252.41	266.49
Zr	171.00	143.40	136.20	154.30	136.60	167.20	143.30	148.60	125.60	141.20	126.90	130.20	111.00	120.40	142.70
Hf	4.51	4.14	3.68	4.23	3.64	4.50	3.97	4.05	3.42	3.78	3.44	3.53	3.16	3.34	3.93
Th	11.58	10.09	8.86	9.87	10.22	11.53	8.92	12.42	12.17	10.20	8.98	9.58	10.01	10.14	10.00
U	2.12	2.20	1.87	2.10	1.86	2.39	2.02	2.49	2.48	2.30	2.24	2.44	2.24	2.26	2.27
Pb	11.20	7.18	8.98	4.58	7.14	10.59	9.42	9.94	12.95	13.22	12.43	12.22	11.73	11.47	13.71
Nb	10.13	8.80	8.07	8.56	8.40	10.10	8.24	8.65	7.03	7.81	14.89	7.99	7.09	7.81	8.04
Y	22.52	20.87	19.88	20.27	20.08	18.52	21.26	21.19	17.84	19.71	20.40	20.37	17.88	19.79	19.44
La	24.34	21.00	20.17	21.33	20.53	21.73	19.17	19.94	17.32	18.41	22.52	19.26	19.90	20.12	19.73
Ce	53.38	49.06	40.01	44.14	42.32	53.30	42.83	45.92	37.70	43.87	40.88	40.60	39.31	41.47	44.03
Pr	5.97	5.52	4.16	4.60	4.39	5.82	5.27	5.10	4.03	4.82	5.12	4.67	4.19	4.80	4.87
Nd	24.07	22.08	19.01	20.75	19.73	23.51	19.03	21.24	18.46	20.01	17.74	19.63	19.01	20.40	20.63
Sm	4.59	4.36	3.91	4.14	4.01	4.44	4.28	4.20	3.76	4.07	4.23	4.09	3.87	4.18	4.22
Eu	0.98	1.01	0.96	0.97	0.93	0.99	1.03	1.03	0.98	0.99	1.13	1.01	0.97	1.00	1.03
Gd	4.20	4.11	3.63	3.86	3.74	3.67	4.17	3.88	3.50	3.73	4.04	3.84	3.62	3.82	3.93
Tb	0.60	0.62	0.56	0.60	0.59	0.55	0.61	0.60	0.53	0.56	0.60	0.55	0.54	0.58	0.57
Dy	3.55	3.60	3.29	3.47	3.35	3.09	3.60	3.52	3.10	3.24	3.31	3.23	3.15	3.28	3.28
Ho	0.73	0.74	0.67	0.71	0.67	0.62	0.75	0.71	0.61	0.64	0.65	0.66	0.62	0.66	0.66
Er	1.96	1.94	1.85	1.94	1.83	1.67	2.05	1.95	1.67	1.78	1.76	1.78	1.70	1.80	1.79
Tm	0.28	0.28	0.31	0.34	0.31	0.26	0.24	0.31	0.29	0.27	0.13	0.25	0.29	0.27	0.27
Yb	2.12	2.09	1.92	2.00	1.91	1.75	2.14	2.05	1.70	1.83	1.91	1.93	1.74	1.84	1.82
Lu	0.34	0.36	0.31	0.32	0.32	0.28	0.35	0.34	0.29	0.30	0.31	0.33	0.29	0.30	0.31

Table 1. Whole rock Major and trace element data from Mt Kinabalu. *Major element data from Sperber (2009).

Lat.	6.1214	6.0733	6.0640	6.0640	6.0766	6.0788	6.0943	6.0741	6.0589	6.0729	6.0705	6.0684	6.0740	6.0738	6.0791	6.0800
Long.	116.5776	116.5575	116.5670	116.5704	116.5758	116.5810	116.5807	116.5790	116.5653	116.5704	116.5703	116.5704	116.6282	116.6168	116.5259	116.5298
Height, m	3025	0	3577	3460	3918	3769	3657	4007	3241.9	3488.96	3611.29	3767.98	3007.82	3126.3	1886.21	2150.33
	Low's Gt	King Gt	King Gt	King Gt	King Gt	King Gt	King Gt	King Gt	King Gt	King Gt	King Gt	King Gt	King Gt	King Gt	King Gt	King Gt
	CS081	SBK123	CS011 c	CS028	CS031	CS066	CS069	CS072	A089c	A128	A129	A131	A236	A237	A282	A285
(wt%)																
SiO_2	59.84	64.04	64.40	64.39	63.59	62.06	64.01	64.96	64.12	64.72	65.53	65.77	63.39	63.01	64.77	62.59
TiO_2	0.67	0.53	0.52	0.52	0.52	0.53	0.55	0.47	0.50	0.47	0.41	0.44	0.51	0.52	0.48	0.54
Al_2O_3	15.02	14.81	14.53	15.13	15.12	15.63	15.30	14.84	14.70	14.88	14.48	14.74	15.06	15.34	14.97	15.06
FeO_{TOT}	6.52	5.04	4.35	4.68	4.89	5.57	5.22	4.64	4.94	4.74	4.14	4.27	5.10	5.10	4.75	5.34
MnO	0.12	0.09	0.07	0.09	0.10	0.12	0.11	0.10	0.09	0.09	0.08	0.09	0.10	0.10	0.10	0.10
MgO	3.87	2.81	2.74	2.60	2.32	2.41	2.82	2.39	2.54	2.40	2.08	2.19	2.64	2.64	2.41	2.78
CaO	6.20	4.86	4.68	4.39	5.25	5.32	3.85	4.53	4.61	4.60	4.18	4.18	4.15	3.60	3.39	4.34
Na_2O	2.48	2.61	2.71	2.69	2.78	2.73	2.21	2.64	2.56	2.72	2.60	2.66	2.36	2.14	2.16	2.40
K_2O	3.40	3.89	4.28	4.65	3.86	4.95	4.51	4.29	4.52	4.40	4.57	4.58	4.34	4.56	4.73	4.50
P_2O_5	0.28	0.20	0.23	0.24	0.26	0.29	0.23	0.21	0.22	0.21	0.18	0.18	0.23	0.24	0.20	0.24
Total	99.75	99.96	99.64	99.90	99.24	100.23	99.39	100.09	99.90	100.32	99.32	100.05	100.02	100.15	100.30	100.03
LOI	0.61	0.52	0.64	1.11	0.77	0.36	1.87	0.49	0.54	0.56	0.60	0.47	1.57	2.33	1.81	1.55
ppm																
Ta	0.70	0.78	0.96	0.82	0.96	0.75	0.81	0.81	0.75	0.64	0.69	0.82	0.73	0.75	0.78	0.68
Sc	25.38	16.83	17.04	13.84	14.24	14.64	15.98	15.56	15.81	14.28	12.29	12.75	15.73	16.03	14.67	17.29
V	211.19	141.75	145.30	115.51	128.08	132.57	112.15	128.95	134.80	123.80	110.70	111.30	134.50	132.90	125.40	147.00
Cr	86.95	58.35	53.81	39.79	31.06	26.75	81.18	46.97	45.75	41.78	37.58	38.94	47.08	47.23	43.60	51.33
Ga	17.65	15.71	16.45	12.25	13.66	13.95	11.85	15.66	16.09	15.76	15.33	15.49	16.10	15.91	16.15	16.56
Co	23.59	15.37	12.67	12.58	10.94	12.59	13.63	14.30	13.29	14.05	12.07	12.74	14.72	15.20	13.62	15.01
Ni	21.19	14.41	12.77	8.78	5.70	4.66	42.73	12.31	12.27	11.72	10.25	11.86	12.83	12.77	11.87	13.62
Cu	59.84	41.01	30.50	21.90	5.70	40.82	8.18	33.83	56.78	26.90	22.19	9.50	18.93	14.43	11.64	16.00
Zn	58.31	41.66	43.02	44.54	30.50	34.30	80.77	44.58	43.56	39.86	32.78	40.89	48.25	49.98	44.44	43.56
Cs	10.08	17.65	12.97	15.04	5.56	9.66	10.34	13.63	18.75	8.65	9.55	17.32	8.88	10.45	13.48	9.93
Rb	119.46	140.99	165.50	166.03	97.37	153.96	144.18	160.97	188.70	158.30	174.60	197.10	155.20	173.70	187.40	167.30
Ba	912.61	883.93	605.60	865.41	677.98	586.81	825.67	661.57	650.50	680.00	623.10	644.00	653.50	720.80	576.50	700.20
Sr	314.28	261.09	283.90	181.39	295.92	293.62	164.05	283.56	296.70	314.10	293.20	288.70	256.80	232.80	195.70	271.00
Zr	140.00	132.80	149.80	132.70	155.10	205.90	137.50	120.10	127.60	135.70	126.70	128.60	140.30	136.10	140.10	142.20
Hf	3.92	3.65	4.28	3.77	4.38	5.63	3.84	3.33	3.45	3.63	3.42	3.68	3.81	3.83	4.03	3.91
Th	10.14	17.71	23.69	13.14	26.48	19.45	14.86	15.58	42.61	21.66	15.98	18.84	18.69	17.14	17.57	9.04
U	2.44	3.83	5.20	3.17	5.18	4.99	3.30	3.57	5.14	4.47	3.87	5.19	3.78	3.50	4.23	2.74
Pb	12.79	13.04	18.06	25.07	13.03	21.02	23.53	19.13	21.76	16.64	16.14	20.48	18.89	20.58	16.74	17.85
Nb	8.01	7.64	8.71	8.76	9.99	8.31	8.79	7.89	8.01	7.17	6.77	7.54	7.86	8.06	7.73	7.57
Y	19.82	15.39	19.69	18.72	23.68	19.73	20.74	15.90	17.37	16.30	15.03	14.99	18.18	18.35	17.36	18.14
La	26.52	16.58	19.70	23.10	39.21	23.75	22.24	20.21	18.95	19.85	17.88	21.09	19.84	23.63	21.35	17.06
Ce	44.20	37.63	50.81	42.66	73.18	51.13	47.99	37.50	37.62	38.99	34.07	38.23	43.21	49.15	45.40	40.82
Pr	5.11	4.07	5.51	4.41	7.69	5.91	5.54	3.88	4.67	4.42	4.05	4.51	4.85	5.21	4.91	4.72
Nd	20.81	16.15	22.13	20.19	30.22	23.75	22.37	17.11	16.30	18.30	13.79	14.96	20.19	21.50	19.84	19.69
Sm	4.22	3.15	4.38	4.11	5.63	4.90	4.49	3.39	3.79	3.66	3.22	3.38	4.03	4.13	3.80	3.98
Eu	1.03	0.78	1.07	0.90	1.16	1.13	0.98	0.87	0.96	0.91	0.87	0.88	0.97	1.00	0.92	0.97
Gd	3.88	2.84	3.88	3.58	4.66	4.25	3.97	2.98	3.42	3.18	2.83	3.10	3.40	3.62	3.33	3.56
Tb	0.57	0.40	0.60	0.55	0.71	0.60	0.57	0.45	0.49	0.48	0.41	0.44	0.51	0.54	0.50	0.52
Dy	3.34	2.45	3.28	3.15	3.90	3.44	3.34	2.57	2.87	2.70	2.37	2.58	2.97	3.08	2.79	3.01
Ho	0.67	0.48	0.67	0.61	0.78	0.68	0.68	0.52	0.56	0.54	0.48	0.51	0.60	0.62	0.58	0.61
Er	1.78	1.29	1.84	1.73	2.13	1.85	1.80	1.43	1.56	1.49	1.30	1.36	1.65	1.73	1.58	1.61
Tm	0.24	0.19	0.29	0.29	0.34	0.27	0.25	0.24	0.16	0.24	0.11	0.12	0.26	0.27	0.25	0.26
Yb	1.94	1.47	1.95	1.85	2.26	2.11	1.96	1.54	1.67	1.63	1.48	1.55	1.74	1.83	1.68	1.76
Lu	0.32	0.25	0.33	0.30	0.36	0.37	0.33	0.26	0.27	0.26	0.24	0.25	0.28	0.30	0.28	0.29

Table 1. (cont.)

Lat.	6.0798	6.0880	6.0705	6.0747	6.0819	6.0665	6.0565	6.0514	6.0555	6.0638	6.0734	6.0747	6.0819	6.0665	6.0565
Long.	116.5350	116.5780	116.5647	116.5697	116.5780	116.5640	116.5646	116.5639	116.5647	116.5739	116.5844	116.5697	116.5780	116.5640	116.5646
Height, m	2443.77	3767	3946.06	3389.22	3805.71	3755.96	0	0	3096	3508.18	3888.38	3389.22	3805.71	3755.96	0
	King Gt	Donkey Gt	Donkey Gt	Donkey Gt	Donkey Gt	Donkey Gt	Paka Pph	Paka Pph	Paka Pph	Paka Pph	Paka Pph	Donkey Gt	Donkey Gt	Donkey Gt	Paka Pph
	A286	CS033	A093	A127	A145	A079	SBK128	SBK130	CS027	A155	A162	A127	A145	A079	SBK128
(wt%)															
SiO_2	64.22	64.06	64.63	63.08	62.56	64.34	64.25	66.53	66.11	64.46	63.17	63.08	62.56	64.34	64.25
TiO_2	0.49	0.48	0.54	0.49	0.52	0.57	0.52	0.45	0.45	0.47	0.50	0.49	0.52	0.57	0.52
Al_2O_3	15.10	14.76	14.70	15.16	15.32	14.89	14.55	14.84	14.71	14.49	14.70	15.16	15.32	14.89	14.55
FeO_{TOT}	4.78	5.04	4.72	4.95	5.03	4.85	5.14	4.48	4.08	4.76	5.09	4.95	5.03	4.85	5.14
MnO	0.10	0.11	0.09	0.10	0.10	0.09	0.10	0.09	0.07	0.10	0.10	0.10	0.10	0.09	0.10
MgO	2.47	2.17	2.60	2.30	2.41	2.75	2.40	1.96	2.02	2.13	2.44	2.30	2.41	2.75	2.40
CaO	3.76	4.73	4.21	5.01	5.08	4.38	4.60	3.45	3.84	4.41	4.70	5.01	5.08	4.38	4.60
Na_2O	2.32	2.77	2.41	2.76	2.62	2.43	2.65	2.08	2.43	2.73	2.67	2.76	2.62	2.43	2.65
K_2O	4.54	5.03	4.29	4.39	4.84	4.26	4.98	4.97	5.30	4.87	4.92	4.39	4.84	4.26	4.98
P_2O_5	0.21	0.25	0.22	0.24	0.25	0.23	0.27	0.22	0.22	0.24	0.25	0.24	0.25	0.23	0.27
Total	100.10	100.25	99.71	99.36	99.80	99.93	100.03	99.57	100.07	99.56	99.59	99.36	99.80	99.93	100.03
LOI	1.59	0.29	0.76	0.33	0.51	0.59	0.20	1.38	0.38	0.38	0.47	0.33	0.51	0.59	0.20
ppm															
Ta	0.68	0.92	0.83	0.62	0.75	0.83	1.01	1.11	0.90	0.82	0.88	0.62	0.75	0.83	1.01
Sc	15.47	15.30	16.01	14.74	15.22	16.11	11.49	9.98	12.89	13.89	15.35	14.74	15.22	16.11	11.49
V	125.80	139.25	117.00	139.30	144.40	119.10	109.92	95.34	122.22	138.00	152.50	139.30	144.40	119.10	109.92
Cr	44.68	27.98	47.09	35.63	35.96	50.97	24.65	22.29	31.93	32.81	43.18	35.63	35.96	50.97	24.65
Ga	15.92	15.96	16.57	16.61	17.40	16.77	13.15	13.15	14.79	15.77	16.46	16.61	17.40	16.77	13.15
Co	14.33	14.41	12.50	14.04	14.02	12.68	9.20	9.55	14.23	13.87	15.40	14.04	14.02	12.68	9.20
Ni	11.87	7.88	11.29	10.00	10.09	12.36	6.99	5.18	9.78	9.73	12.53	10.00	10.09	12.36	6.99
Cu	14.52	23.21	16.69	26.39	31.78	26.31	105.34	47.95	143.70	35.64	44.41	26.39	31.78	26.31	105.34
Zn	42.65	44.63	59.55	40.96	32.48	58.49	26.23	30.63	31.11	39.30	36.46	40.96	32.48	58.49	26.23
Cs	12.66	12.25	17.95	8.15	7.87	13.81	7.90	11.14	10.74	16.77	12.16	8.15	7.87	13.81	7.90
Rb	189.50	202.78	178.60	150.80	182.00	177.10	175.83	170.41	233.82	224.00	221.80	150.80	182.00	177.10	175.83
Ba	679.00	567.97	561.90	646.80	675.60	591.90	511.13	469.77	441.85	463.70	579.50	646.80	675.60	591.90	511.13
Sr	244.30	328.89	302.80	360.20	361.20	322.80	270.88	209.50	300.51	344.00	377.30	360.20	361.20	322.80	270.88
Zr	130.40	134.70	161.60	138.90	154.30	179.90	124.30	130.90	117.80	118.60	135.90	138.90	154.30	179.90	124.30
Hf	3.67	4.07	4.62	3.80	4.19	4.77	3.89	4.09	3.52	3.43	4.05	3.80	4.19	4.77	3.89
Th	16.97	24.40	20.90	17.42	17.01	14.69	27.64	30.93	28.21	10.54	26.72	17.42	17.01	14.69	27.64
U	4.00	6.14	4.10	3.66	2.73	3.14	6.46	5.80	4.82	3.94	6.30	3.66	2.73	3.14	6.46
Pb	16.41	20.45	24.38	16.22	13.65	21.75	25.55	23.71	17.83	19.31	22.55	16.22	13.65	21.75	25.55
Nb	7.57	8.80	9.76	7.49	7.59	10.29	9.00	9.74	8.19	8.33	8.85	7.49	7.59	10.29	9.00
Y	16.82	20.18	21.73	20.01	19.24	22.27	18.11	22.11	18.19	18.70	18.91	20.01	19.24	22.27	18.11
La	20.48	22.70	26.84	17.73	19.40	24.07	19.98	30.43	28.31	17.42	24.71	17.73	19.40	24.07	19.98
Ce	46.25	47.97	60.79	44.21	41.95	54.53	48.93	57.24	54.11	36.46	55.81	44.21	41.95	54.53	48.93
Pr	4.87	5.62	6.67	5.08	5.17	6.63	5.85	6.70	5.55	4.81	6.23	5.08	5.17	6.63	5.85
Nd	19.83	22.74	27.12	22.00	18.05	23.68	24.13	26.84	24.28	17.98	25.34	22.00	18.05	23.68	24.13
Sm	3.82	4.60	5.24	4.38	4.21	5.22	4.97	5.14	4.45	4.37	4.97	4.38	4.21	5.22	4.97
Eu	0.93	1.03	1.13	1.09	1.08	1.21	1.13	1.16	1.00	1.07	1.13	1.09	1.08	1.21	1.13
Gd	3.30	3.94	4.45	3.84	3.83	4.63	4.16	4.21	3.67	3.94	4.00	3.84	3.83	4.63	4.16
Tb	0.49	0.55	0.66	0.57	0.55	0.66	0.56	0.60	0.52	0.51	0.56	0.57	0.55	0.66	0.56
Dy	2.77	3.04	3.73	3.23	3.12	3.77	3.13	3.37	2.90	3.00	3.14	3.23	3.12	3.77	3.13
Ho	0.56	0.62	0.76	0.67	0.62	0.75	0.63	0.68	0.59	0.59	0.63	0.67	0.62	0.75	0.63
Er	1.54	1.74	2.08	1.80	1.67	2.14	1.69	1.87	1.66	1.62	1.71	1.80	1.67	2.14	1.69
Tm	0.25	0.25	0.32	0.29	0.16	0.24	0.25	0.27	0.29	0.14	0.28	0.29	0.16	0.24	0.25
Yb	1.65	2.05	2.20	1.88	1.90	2.26	1.93	2.19	1.83	1.82	1.90	1.88	1.90	2.26	1.93
Lu	0.27	0.34	0.36	0.31	0.30	0.36	0.33	0.37	0.31	0.29	0.30	0.31	0.30	0.36	0.33

Table 1. (cont.)

Lat.	6.0514	6.0555	6.0638	6.0734	6.0665	6.0814	6.0793	6.0800	6.0723	6.0494	6.0733	6.0595	6.0595	6.132023	6.03124	6.070546
Long.	116.5639	116.5647	116.5739	116.5844	116.5815	116.5867	116.5909	116.5999	116.6012	116.5891	116.6143	116.5936	116.5940	116.5698	116.5483	116.5642
Height, m	0	3096	3508.18	3888.38	3769	3332	3513	3133	3413	2715	3134	2393	2393	2239	1874	3968
	Paka Pph	Paka Pph	Paka Pph	Paka Pph	Mes Pph	Mes Pph	Mes Pph	Mes Pph	Mes Pph	Mes Pph	Mes Pph	Mes Pph	Mes Pph	Quartzite	Sst	Xenolith
	SBK130	CS027	A155	A162	A152	A167	A170	A172	A173	A190	A241	CS055	CS056	A221	A291	A098
(wt%)																
SiO_2	66.53	66.11	64.46	63.17	63.61	64.87	63.32	62.37	63.01	60.38	63.77	64.04	64.54	77.95	83.81	83.42
TiO_2	0.45	0.45	0.47	0.50	0.51	0.48	0.52	0.52	0.47	0.53	0.49	0.48	0.50	0.51	0.46	0.20
Al_2O_3	14.84	14.71	14.49	14.70	14.45	14.36	14.55	15.10	15.43	15.18	14.91	15.19	15.52	10.62	8.40	8.08
FeO_{TOT}	4.48	4.08	4.76	5.09	5.12	4.80	5.16	5.18	4.72	5.87	5.01	4.40	4.37	4.15	1.75	1.26
MnO	0.09	0.07	0.10	0.10	0.11	0.11	0.11	0.11	0.10	0.12	0.11	0.08	0.07	0.05	0.01	0.01
MgO	1.96	2.02	2.13	2.44	2.41	2.38	2.48	2.35	2.19	2.58	2.24	2.10	2.03	1.59	0.64	0.99
CaO	3.45	3.84	4.41	4.70	4.60	4.40	4.70	4.88	3.96	5.58	4.56	4.54	3.37	0.03	-0.05	1.90
Na_2O	2.08	2.43	2.73	2.67	2.66	2.51	2.56	2.76	2.64	2.76	2.72	2.80	2.50	0.21	1.79	1.37
K_2O	4.97	5.30	4.87	4.92	4.82	4.70	4.81	4.80	5.13	4.82	4.71	4.67	6.16	2.03	1.03	1.49
P_2O_5	0.22	0.22	0.24	0.25	0.25	0.23	0.25	0.26	0.23	0.31	0.24	0.22	0.24	0.06	0.07	0.04
Total	99.57	100.07	99.56	99.59	99.49	100.06	99.55	99.41	99.43	99.21	99.96	100.08	99.79	99.87	99.70	99.88
LOI	1.38	0.38	0.38	0.47	0.38	0.69	0.50	0.50	1.02	0.43	0.64	1.06	1.68	2.21	1.60	
ppm																
Ta	1.11	0.90	0.82	0.88	1.00	0.81	0.76	0.77	0.59	0.45	0.80	0.59	0.61	0.75	0.56	0.31
Sc	9.98	12.89	13.89	15.35	15.17	14.47	15.93	14.90	14.12	16.24	14.88	14.02	10.44	8.39	4.94	3.77
V	95.34	122.22	138.00	152.50	146.10	139.40	153.50	151.30	134.20	177.70	145.70	135.70	92.37	67.99	49.69	29.08
Cr	22.29	31.93	32.81	43.18	41.46	44.92	49.28	37.89	39.13	28.72	35.15	36.54	20.51	51.51	29.31	25.95
Ga	13.15	14.79	15.77	16.46	16.72	15.97	16.07	17.40	16.70	17.01	16.87	16.62	13.17	11.48	8.32	8.00
Co	9.55	14.23	13.87	15.40	15.38	14.46	15.63	15.27	13.94	17.80	14.80	14.21	8.93	7.79	2.04	4.82
Ni	5.18	9.78	9.73	12.53	12.38	11.87	13.34	11.06	11.20	9.39	10.52	10.00	2.43	21.91	7.25	34.96
Cu	47.95	143.70	35.64	44.41	51.80	206.10	1.96	57.62	81.57	54.91	53.99	262.78	347.06	19.44	7.20	6.37
Zn	30.63	31.11	39.30	36.46	46.21	42.32	44.33	49.67	50.75	49.10	52.40	35.21	19.91	44.64	32.70	10.61
Cs	11.14	10.74	16.77	12.16	12.99	12.39	9.55	12.42	10.94	8.89	13.41	7.34	8.36	6.79	3.77	9.03
Rb	170.41	233.82	224.00	221.80	225.00	203.00	216.60	209.60	216.90	182.20	219.70	238.44	221.90	96.26	46.23	111.50
Ba	469.77	441.85	463.70	579.50	446.30	368.30	460.90	560.10	610.70	729.00	446.10	379.01	450.60	201.90	141.20	137.40
Sr	209.50	300.51	344.00	377.30	343.20	335.40	365.50	425.20	410.10	438.30	386.30	419.03	334.79	38.71	35.01	133.90
Zr	130.90	117.80	118.60	135.90	114.60	133.70	120.50	135.70	117.20	134.50	118.40	107.00	99.45	230.80	274.80	24.11
Hf	4.09	3.52	3.43	4.05	3.34	3.76	3.42	3.86	3.28	3.48	3.50	3.03	2.83	6.08	7.13	0.67
Th	30.93	28.21	10.54	26.72	19.12	15.11	28.49	25.16	21.88	22.20	28.05	26.15	26.17	9.16	8.74	5.12
U	5.80	4.82	3.94	6.30	6.48	3.92	5.01	4.53	4.41	3.61	5.72	5.20	4.95	2.08	2.01	1.15
Pb	23.71	17.83	19.31	22.55	24.41	20.32	23.42	23.94	26.45	20.60	25.46	19.64	22.82	6.23	7.96	7.59
Nb	9.74	8.19	8.33	8.85	9.32	8.02	7.94	8.65	7.04	5.82	8.38	6.75	6.69	8.85	6.47	3.25
Y	22.11	18.19	18.70	18.91	20.02	17.93	16.92	19.62	16.67	13.81	19.24	14.53	13.87	19.29	20.23	10.26
La	30.43	28.31	17.42	24.71	21.62	25.69	24.77	25.95	25.01	20.53	27.37	20.97	26.07	20.54	22.52	14.53
Ce	57.24	54.11	36.46	55.81	46.64	49.55	51.36	57.97	51.57	40.90	58.16	47.20	46.94	42.96	39.21	27.94
Pr	6.70	5.55	4.81	6.23	5.92	5.99	5.69	6.54	5.76	4.48	6.59	5.04	4.96	5.27	5.48	3.43
Nd	26.84	24.28	17.98	25.34	21.11	21.10	23.72	27.44	23.72	18.91	27.50	22.24	22.09	19.69	21.09	12.53
Sm	5.14	4.45	4.37	4.97	4.83	4.75	4.66	5.35	4.65	3.72	5.30	4.38	4.07	3.87	4.37	2.31
Eu	1.16	1.00	1.07	1.13	1.11	1.08	1.08	1.19	1.17	1.08	1.17	1.08	1.07	0.60	0.92	0.67
Gd	4.21	3.67	3.94	4.00	4.31	4.31	3.74	4.19	3.69	3.07	4.14	3.44	3.15	3.57	4.39	2.02
Tb	0.60	0.52	0.51	0.56	0.57	0.56	0.52	0.59	0.52	0.43	0.57	0.46	0.44	0.58	0.64	0.31
Dy	3.37	2.90	3.00	3.14	3.12	3.06	2.86	3.18	2.81	2.31	3.20	2.53	2.36	3.32	3.42	1.71
Ho	0.68	0.59	0.59	0.63	0.62	0.59	0.57	0.62	0.57	0.45	0.64	0.51	0.46	0.70	0.70	0.33
Er	1.87	1.66	1.62	1.71	1.69	1.59	1.53	1.71	1.53	1.21	1.71	1.33	1.27	1.96	1.90	0.89
Tm	0.27	0.29	0.14	0.28	0.15	0.14	0.24	0.28	0.24	0.19	0.27	0.23	0.22	0.32	0.30	0.14
Yb	2.19	1.83	1.82	1.90	1.91	1.81	1.60	1.88	1.63	1.26	1.84	1.44	1.33	2.07	1.94	0.84
Lu	0.37	0.31	0.29	0.30	0.31	0.30	0.27	0.31	0.28	0.22	0.30	0.24	0.23	0.35	0.33	0.13

Table 1. (cont.)

													$\delta^{18}O_{V\text{-}SMOW}$ (‰)						
Lithology	Sample	$^{87}Sr/^{86}Sr_m$	2SE	$^{143}ND/^{144}Nd_m$	2SE	$^{206}Pb/^{204}Pb_m$	2SE	$^{207}Pb/^{204}Pb_m$	2SE	$^{208}Pb/^{204}Pb_m$	2SE	Hornblende	SD	Quartz	SD	Biotite	SD	Whole Rock $\delta^{18}O$ (‰)*
Alexandra Tn/Gd	A042	0.707888	11	0.512435	08	18.7761	06	15.6811	07	39.0200	34							
Alexandra Tn/Gd	A047	0.707640	10	0.512482	07	18.7729	11	15.6823	10	39.0192	43	4.8	0.4	8.3	0.1	-1.3	0.4	6.9
Alexandra Tn/Gd	A049	0.707939	07	0.512449	11	18.7763	06	15.6791	07	39.0151	31	8.2	0.14	9.8	0.3			9.1
Alexandra Tn/Gd	A054	0.707536	18	0.512488	04	18.7732	12	15.6780	12	39.0094	31	6.6	0.0	10.3	0.1	4.9	0.3	8.4
Low's Gt	A046											7.0	0.4					8.3
Low's Gt	A218	0.706805	18	0.512548	06	18.7477	09	15.6716	09	38.9647	30	7.2	0.1	10.2	0.1	5.9	0.4	8.5
Low's Gt	SBK122	0.706989	09	0.512505	08	18.7463	06	15.6698	08	38.9574	34							
King Gt	A236	0.706702	12	0.512508	08	18.7387	08	15.6676	08	38.9488	47							
King Gt	A282	0.706849	08	0.512493	10	18.7397	08	15.6685	07	38.9460	27	7.0	0.1	9.8	0.4	0.3	0.3	8.5
Donkey Gt	A093	0.707595	16	0.512443	09	18.7518	12	15.6731	12	38.9766	41	8.1	0.9	10.0	0.1			9.3
Donkey Gt	A096											7.5	0.1					9.0
Donkey Gt	A127	0.706542	17	0.512584	04	18.7366	10	15.6683	09	38.9451	32	6.6	0.3	9.6	0.1			8.1
Paka Pph	A162	0.706644	09	0.512503	10	18.7363	06	15.6670	08	38.9371	35	6.8	0.0	10.1	0.1			8.6
Paka Pph	A290b	0.706938	11	0.512500	08	18.7264	06	15.6635	07	38.9163	27							
Paka Pph	CS027	0.706682	16	0.512533	05	18.7474	08	15.6724	07	38.9699	27	5.4	0.8					7.2
Mesilau Pph	A172	0.706642	10	0.512499	10	18.7337	07	15.6659	08	38.9351	32							
Mesilau Pph	A198	0.706462	08	0.512526	08	18.7288	10	15.6669	10	38.9306	33	7.2	0.4	9.4	0.4			8.4
Mesilau Pph	A239											6.7	0.2					7.9
Mesilau Pph	A241	0.706646	09	0.512498	07	18.7373	08	15.6664	07	38.9409	29							
Mesilau Pph	CS055	0.706653	09	0.512507	07	18.7417	08	15.6687	08	38.9491	32							
Xenolith	A098	0.710785	17	0.512259	09	18.7482	15	15.6729	14	38.9582	45							
Quartzite	A221	0.715460	72	0.512387	27	18.8302	11	15.6966	11	39.1173	34							
Quartzite	A291	0.713415	75	0.512413	06	18.8495	10	15.6903	09	39.1089	26							

Table 2. Isotopic data from Mt Kinabalu. *Whole rock $\delta^{18}O$ calculated from hornblende $\delta^{18}O$ as detailed in the text.

Two-Component Partition Coefficients		Min	Max	Mean	SD	n	Kinabalu value
Plagioclase	$(Al^{Plag} \times Si^{Liq}) / (Si^{Plag} \times Al^{Liq})$	1.79	4.20	2.46	0.51	36	2.46
Pl. (52-57 % SiO_2)	$(Al^{Plag} \times Si^{Liq}) / (Si^{Plag} \times Al^{Liq})$	1.79	2.22	2.01	0.18	5	2.01
Pl. (57-63 % SiO_2)	$(Al^{Plag} \times Si^{Liq}) / (Si^{Plag} \times Al^{Liq})$	1.90	2.85	2.31	0.31	16	2.31
Pl. (>63 % SiO_2)	$(Al^{Plag} \times Si^{Liq}) / (Si^{Plag} \times Al^{Liq})$	2.05	4.20	2.80	0.58	14	2.80
Plagioclase	$(K^{Plag} \times Na^{Liq}) / (Na^{Plag} \times K^{Liq})$	0.03	0.19	0.09	0.04	36	0.09
Hornblende	$(Fe^{Hbl} \times Mg^{Liq}) / (Mg^{Hbl} \times Fe^{Liq})$	0.23	0.53	0.36	0.07	28	0.25
Hornblende	$(Al^{Hbl} \times Si^{Liq}) / (Si^{Hbl} \times Al^{Liq})$	0.26	1.60	1.13	0.27	28	0.60
Clinopyroxene	$(Fe^{Cpx} \times Mg^{Liq}) / (Mg^{Cpx} \times Fe^{Liq})$	0.20	0.51	0.28	0.07	23	0.28
Clinopyroxene	$(Al^{Cpx} \times Si^{Liq}) / (Si^{Cpx} \times Al^{Liq})$	0.12	0.68	0.27	0.18	23	0.27
Orthopyroxene	$(Fe^{Opx} \times Mg^{Liq}) / (Mg^{Opx} \times Fe^{Liq})$	0.20	0.53	0.28	0.08	15	0.28
Orthopyroxene	$(Al^{Opx} \times Si^{Liq}) / (Si^{Opx} \times Al^{Liq})$	0.07	0.52	0.19	0.16	15	0.19
Olivine	$(Fe^{Ol} \times Mg^{Liq}) / (Mg^{Ol} \times Fe^{Liq})$	0.24	0.33	0.28	0.03	14	0.28
Biotite	$(Al^{Bt} \times Si^{Liq}) / (Si^{Bt} \times Al^{Liq})$	2.52	2.52	2.52		1	2.52
Garnet	$(Fe^{Cpx} \times Mg^{Liq}) / (Mg^{Cpx} \times Fe^{Liq})$	0.60	1.59	0.97	0.28	16	0.97

Table 3. Two-component major element partition coefficients determined from experimental data (Grove *et al.*, 2003; Alonso-Perez *et al.*, 2008; Nandedkar *et al.*, 2014).

Fractionating phases	Melt SiO_2, wt.%			Bulk Cumulate, %			
	52-57	57-63	>63	Alexandra	Low's	King	Other units
Ol							
Cpx	42			11.7-14.9	19.4-23.9	13.8-17.3	13.1-21.1
Opx	42			11.7-14.9	19.4-23.9	13.8-17.3	13.1-21.1
Hbl		30	30	19.2-21.5	12.8-16.0	17.5-20.0	14.8-20.5
Pl	11	65	65	45.5-49.7	34.0-39.7	42.4-46.9	37.6-47.8
Kfs							
Bt							
Ap	0.5	0.5	0.5	0.5	0.5	0.5	0.5
Mag	1.5	1.5	1.5	1.5	1.5	1.5	1.5
Ilm	3.5	3.5	3.5	3.5	3.5	3.5	3.5
Zrn		0.02	0.02	0.01	0.01	0.01	0.01
Rt							
Grt							
F				0.59-0.73	0.72-0.78	0.54-0.66	0.5-0.74
r, $M_{assimilated}/M_{crystallised}$				0.56-0.72	0.65-0.73	0.4-0.57	0.36-0.66
ρ, total $M_{assimilated}/M^0_{melt}$				0.22-0.29	0.16-0.21	0.23-0.25	0.2-0.25

Table 4. Fractionating phases, parameters and outputs of the EME-AFC modelling of the Alexandra Tonalite/Granodiorite, the Low's Granite and the King Granite.